EUROPEAN ORGANIZATION FOR NUCLEAR RESEARCH

CERN-PH-EP/2005-XXX

June 6, 2005

Search for Neutral MSSM Higgs Bosons at LEP

ALEPH, DELPHI, L3 and OPAL Collaborations
The LEP Working Group for Higgs Boson Searches

Abstract

The four LEP collaborations, ALEPH, DELPHI, L3 and OPAL, have searched for neutral Higgs bosons which are predicted within the framework of the Minimal Supersymmetric Model (MSSM). The data of the four collaborations are statistically combined and examined for their consistency with the background hypothesis and for a possible Higgs boson signal. The combined LEP data show no significant excess of events which would indicate the production of Higgs bosons. The search results are thus used to set upper bounds on the cross sections of various Higgs-like event topologies. The results are interpreted within the MSSM for a number of "benchmark" models, including CP-conserving and CP-violating scenarios. In all cases these interpretations lead to large exclusions in the theoretical MSSM parameter space. In some scenarios absolute limits are set on the masses of neutral Higgs bosons.

To be submitted to Eur. Phys. Journal C

Comments to Peter.Igo-Kemenes@cern.ch

1 Introduction

One of the outstanding questions in particle physics is that of electroweak symmetry breaking and the origin of mass. These are believed to be generated by the Higgs mechanism [1]. Fundamental scalar Higgs fields interact with each other, thereby acquiring nonzero vacuum expectation values and spontaneously breaking the electroweak symmetry. Gauge bosons and fermions obtain their masses by interacting with the resulting vacuum Higgs fields. Associated with this description is the existence of massive scalar particles, Higgs bosons.

The Standard Model [2] requires one Higgs field doublet and predicts a single neutral Higgs boson of unknown mass. Despite extensive searches at LEP and elsewhere, the Standard Model Higgs boson could not be detected so far and a lower bound of 114.4 GeV/c^2 has been established for its mass [3], at the 95% confidence level (c.l.).

Supersymmetric (SUSY) extensions of the Standard Model [4] are of interest since they provide a consistent framework for the unification of the gauge interactions at a high energy scale and for the stability of the universe at the electroweak scale. Moreover, their predictions are compatible with existing high-precision data [5].

The Minimal Supersymmetric Standard Model (MSSM) (reviewed e.g. in [6]) is the SUSY extension with minimal new particle content. It introduces two Higgs field doublets, and predicts the existence of three neutral and two charged Higgs bosons. The lightest of the neutral Higgs bosons is predicted to have a mass less than about 140 GeV/c^2 after radiative corrections [7]. This prediction provided a strong motivation for the searches at LEP energies.

Most of the experimental investigations carried out in the past at LEP and elsewhere were interpreted in MSSM scenarios which assume CP conservation in the Higgs sector. In such scenarios the three neutral Higgs bosons are CP eigenstates: h and H are CP-even and A is CP-odd. However, CP violation in the Higgs sector cannot be a priori excluded [8]. Scenarios with CP violation are theoretically appealing since they provide one of the ingredients needed to explain the observed cosmic matter-antimatter asymmetry. The observed size of CP violation in the Standard Model is not sufficient to drive this asymmetry. In the MSSM, however, substantial CP-violating effects can be induced by radiative corrections, especially from third generation scalar-quarks [9]. In the CP-violating scenario the three neutral Higgs mass eigenstates, H_1, H_2 and H_3, are mixtures of CP-even and CP-odd fields. The Higgs boson production and decay properties may therefore be widely different and, consequently, the experimental exclusions published so far for the CP-conserving MSSM scenario may be invalidated by CP-violating effects. The effects of CP violation have recently been studied experimentally [10].

In this paper we describe the results of a statistical combination of the searches carried out by the four LEP collaborations [10–13]. These searches include all LEP2 data up to the highest LEP energy, 209 GeV; in the case of Refs. [10, 12] they also include the LEP1 data collected at energies in the vicinity of 91 GeV (the Z boson resonance). The combined LEP data show no significant signal for Higgs boson production. The search results are thus used to set upper bounds on topological cross sections for a number of Higgs-like final states and they are interpreted in a set of representative MSSM "benchmark" models, with and without CP-violating effects included in the Higgs sector.

2 The MSSM framework

The LEP searches and their present combination are interpreted in a constrained MSSM model. At tree level, two parameters are sufficient - besides the known parameters of the Standard Model fermion and gauge sectors - to fully describe the Higgs sector. A convenient choice is one Higgs boson mass (m_{A} is chosen in CP-conserving and $m_{\mathrm{H}^\pm}$ in CP-violating scenarios), and the ratio $\tan\beta = v_2/v_1$ of the vacuum expectation values of the two Higgs fields (v_2 and v_1 refer to the fields which couple to the up- and down-type fermions). Additional parameters, M_{SUSY}, M_2, μ, A and $m_{\tilde{\mathrm{g}}}$, enter at the level of radiative corrections. M_{SUSY} stands for the energy scale of SUSY breaking; it is a common mass for all scalar-fermions (sfermions) at the electroweak scale. Similarly, M_2 is a common gaugino mass at the electroweak scale. The parameter μ is the strength of the supersymmetric Higgs mixing, A a common trilinear Higgs-squark coupling and $m_{\tilde{\mathrm{g}}}$ the gluino mass. Three of these parameters define the stop and sbottom mixing parameters $X_t = A - \mu\cot\beta$ and $X_b = A - \mu\tan\beta$. In the CP-violating scenario the complex phases related to A and $m_{\tilde{\mathrm{g}}}$ are supplementary parameters. In addition to all these MSSM parameters, the top quark mass has also a strong impact on the results through radiative corrections. In this paper it is fixed at m_{t}=179.4 GeV/c^2 (which is within the current experimental range of 178.0±4.3 GeV/c^2 [14]); the dependence of the results on other values of the top quark mass is discussed in the results sections.

The combined LEP data are compared to the predictions of a number of MSSM "benchmark" models [16]. Within each of these models, the two tree-level parameters, $\tan\beta$ and m_{A} (in the CP-conserving scenario) or $m_{\mathrm{H}^\pm}$ (in the CP-violating scenario) are scanned over broad ranges while the other parameters are set to fixed values. Each scan point thus represents a specific MSSM model. The ranges of the scanned parameters and the values of the fixed parameters are listed in Table 1. The first three models represent benchmarks for the CP-conserving scenario while the last model, labeled *CPX*, is a benchmark model for the CP-violating scenario.

The scan range of $\tan\beta$ is limited due to the following considerations. For values of $\tan\beta$ below the indicated lower bounds the calculations of the observables in the Higgs sector (masses, cross sections and decay branching ratios) become uncertain while for values above the upper bounds the decay width of the Higgs bosons may become larger than the experimental mass resolution (typically of a few GeV/c^2) and the modeling of the signal efficiencies becomes inaccurate.

For a given scan point, the observables in the Higgs sector are calculated using two theoretical approaches. The FeynHiggs 2.0 code [19] is based on a two-loop diagrammatic approach and uses the OS renormalization scheme while SUBHPOLE and its CP-violating variant CPH [17] are based on a one-loop renormalization group improved calculation [20] and uses the $\overline{\mathrm{MS}}$ scheme. Both calculations give consistent results although small differences naturally exist.

Benchmark parameters						
	(1) *no-mixing*	(2) m_{h}-*max*	(3) large-μ	(4) *gluophobic*	(5) *larg*-α_{eff}	(6) *CPX*
Parameters varied in the scan						
$\tan\beta$	0.4–40	0.4–40	1–50	0.4–40	0.4–40	0.6–40
m_{A} (GeV)	4–1000	4–1000	4–400	4–1000	4–1000	–
$m_{\mathrm{H}^\pm}$ (GeV)	–	–	–	–	–	4–1000
Fixed parameters						
M_{SUSY} (GeV)	1000	1000	400	350	800	500
M_2 (GeV)	200	200	400	300	500	200
μ (GeV)	-200	-200	1000	300	2000	2000
$m_{\tilde{\mathrm{g}}}$ (GeV)	800	800	200	500	500	1000
X_t (GeV)	0	$\sqrt{6}\,M_{\mathrm{SUSY}}$	-300	-750	-1100	$A-\mu\cot\beta$
A (GeV)	$X_t+\mu\cot\beta$	$X_t+\mu\cot\beta$	$X_t+\mu\cot\beta$	$X_t+\mu\cot\beta$	$X_t+\mu\cot\beta$	1000
$\arg A$, $\arg m_{\tilde{\mathrm{g}}}$	-	-	-	-	-	90°

Table 1: *Parameters of the main benchmark scenarios investigated. The values of* $\tan\beta$ *and the mass parameters* m_{A} *(in the CP-conserving scenario) and* $m_{\mathrm{H}^\pm}$ *(in the CP-violating scenario) are scanned within the indicated ranges. The top mass is fixed at 179.3* GeV/c^2*. For the definition of* A *and* X_t *the* $\overline{\mathrm{MS}}$ *renormalisation scheme is adopted.*

The largest difference occurs in the *CPX* scenario at large $\tan\beta$ where the FeynHiggs calculation predicts a higher Higgsstrahlung cross section than the CPH calculation.

In the CP-conserving case, the FeynHiggs calculation is retained for the presentation of the results since it yields slightly more conservative results (the theoretically allowed parameter space is wider) than SUBHPOLE. Also, FeynHiggs is preferred on theoretical grounds since its radiative corrections are more detailed than those of SUBHPOLE.

In the CP-violating case, neither of the two existing calculations is preferred a priori on theoretical grounds. While FeynHiggs contains more advanced one-loop corrections, the CPH code is more precise at the two-loop level. We therefore opted for a solution where, in each scan point, the calculation yielding the more conservative result (weaker exclusion) is retained. However, the effect of using either one or the other calculation is also discussed.

All codes are implemented in a modified version of the HZHA program package [21] which takes into account initial-state radiation and the interference between identical final states from Higgsstrahlung and boson fusion processes.

2.1 The CP-conserving scenario

Assuming CP invariance, the spectrum of MSSM Higgs bosons consists of two CP-even neutral scalars h and H (h is defined to be the lighter of the two), one CP-odd neutral scalar A, and one pair of charged Higgs bosons $\mathrm{H}^{\pm}$. The following ordering of masses is valid at tree level: $m_{\mathrm{h}}<(m_{\mathrm{Z}},\, m_{\mathrm{A}})<m_{\mathrm{H}}$ and $m_{\mathrm{W}^{\pm}}<m_{\mathrm{H}^{\pm}}$. This ordering may be substantially modified by radiative corrections [7], the largest contribution arising from the incomplete cancellation between top and scalar-top (stop) loops. The corrections affect mainly the neutral Higgs boson masses and decay branching ratios.

In $\mathrm{e^+e^-}$ collisions at LEP energies, the main production processes of h, H and A are Higgsstrahlung, $\mathrm{e^+e^-}\to$hZ and HZ (if kinematically possible), and pair production, $\mathrm{e^+e^-}\to$hA and HA (if kinematically possible). Fusion processes, $\mathrm{e^+e^-}\to$ (WW$\to$ H)$\nu_{\mathrm{e}}\bar{\nu}_{\mathrm{e}}$ and $\mathrm{e^+e^-}\to$ (ZZ$\to$ H)$\mathrm{e^+e^-}$, play a marginal role at LEP energies. The cross sections for Higgsstrahlung and pair production can be expressed in terms of the Standard Model Higgs boson cross section $\sigma^{SM}_{\mathrm{HZ}}$. The following expressions hold for h and for A:

$$\sigma_{\mathrm{hZ}} = \sin^2(\beta-\alpha)\ \sigma^{SM}_{\mathrm{HZ}} \tag{1}$$

$$\sigma_{\mathrm{hA}} = \cos^2(\beta-\alpha)\bar{\lambda}\ \sigma^{SM}_{\mathrm{HZ}}. \tag{2}$$

Here α is the mixing angle which diagonalises the CP-even Higgs mass matrix (it can be expressed in terms of m_{A} and $\tan\beta$) and $\bar{\lambda}$ is a kinematic factor given by

$$\bar{\lambda} = \lambda^{3/2}_{\mathrm{Ah}}/[\lambda^{1/2}_{\mathrm{Zh}}(12M^2_{\mathrm{Z}}/s+\lambda_{\mathrm{Zh}})] \tag{3}$$

with

$$\lambda_{ij} = [1-(m_i+m_j)^2/s][1-(m_i-m_j)^2/s]. \tag{4}$$

The Higgsstrahlung and pair production cross sections are complementary, as can be seen from Eqs. (1) and (2). Typically, the process $\mathrm{e^+e^-}\to$ hZ is more abundant at small $\tan\beta$ and $\mathrm{e^+e^-}\to$ hA at large $\tan\beta$ but the latter process can be suppressed also by the kinematic factor $\bar{\lambda}$. The cross sections for the heavy scalar boson H are obtained by interchanging $\sin^2(\beta-\alpha)$ and $\cos^2(\beta-\alpha)$ in Eqs. (1) and (2) and replacing the index h by H in Eq. (3).

The following decay features are relevant to the neutral MSSM Higgs bosons. The h boson will decay mainly to fermion pairs since its mass is below threshold for the processes h$\to$ WW and ZZ although, for particular choices of parameters, the fermionic final states may be strongly suppressed. The A boson also decays predominantly to fermion pairs, independently of its mass, since its coupling to vector bosons is zero at leading order. For $\tan\beta>1$, decays of h and A to $\mathrm{b\bar{b}}$ and $\tau^+\tau^-$ pairs are preferred while the decays to $\mathrm{c\bar{c}}$ and gluon pairs are suppressed. Decays to $\mathrm{c\bar{c}}$ may become important for $\tan\beta<1$. The decay h$\to$AA may be dominant if kinematically allowed [15]. Other decays can involve SUSY particles such as sfermions, charginos or invisible neutralinos, thus requiring special search strategies.

The following benchmark scenarios are examined in the CP-conserving case.

2.1.1 The m_{h}-*max* scenario

In the m_{h}-*max* scenario the stop mixing parameter is set to a large value, $X_t = \sqrt{6}\ M_{\mathrm{SUSY}}$ using the $\overline{\mathrm{MS}}$ renormalisation scheme. The parameters are listed in Table 1. This model is designed to maximise the theoretical upper bound of $m_{\rm h}$ for a given $\tan\beta$ and fixed $m_{\rm t}$ and M_{SUSY} (uncertainties from unknown higher-order corrections are ignored). This model thus provides a widest parameter space and therefore the most conservative exclusion limits among all the scenarios studied.

- (a) We also examine a variant of this scenario where the sign of μ flipped, which is favoured by presently available results on on $(g-2)_\mu$ [29].
- (b) Furthermore, we examine the case where, besides the sign of μ, the sign of the mixing parameter $X_{\rm t}$ is also flipped. This choice of parameters gives better agreement with measurements of the branching ratio BR(b$\rightarrow$ sγ) [30].

2.1.2 The *no-mixing* scenario

In the *no-mixing* scenario the stop mixing parameter $X_{\rm t}$ is set to zero, giving rise to a relatively restricted MSSM parameter space. The other parameters are listed in Table 1.

- (a) We also examine a variant of this scenario where the sign of μ is flipped and M_{SUSY} is raised to 2 TeV. This choice of parameters gives better agreement with recent measurements on $(g-2)_\mu$ [29]. In this case $\tan\beta$ is scanned only from 0.7 upwards due to numerical instabilities in the diagonalisation of the mass matrix for lower values.

2.1.3 "Technical" scenarios

Special models are designed to illustrate choices of MSSM parameters for which the detection of Higgs bosons at LEP and at the future pp collider LHC is expected to be difficult a priori due to the suppression of some main discovery channels.

- The *large-μ* scenario is constructed in such a way that the h boson is kinematically accessible at LEP for all scan points ($m_{\rm h}$<110 GeV/c^2) but the decay of h to b$\bar{\rm b}$, on which most of the LEP searches are based, is strongly suppressed. For many of the scan points the decay h$\rightarrow \tau^+\tau^-$ is also suppressed such that the dominant decay modes are h$\rightarrow$ c$\bar{\rm c}$, gg and W$^+$W$^-$. The detection of Higgs bosons thus relies mainly on flavour- and decay-mode-independent searches. Moreover, in some of the scan points the Higgsstrahlung is suppressed altogether by a small value of $\sin^2(\beta-\alpha)$; In these cases, however, the heavy neutral scalar H is within reach ($m_{\rm H}$ < 111 GeV/c^2) and the cross section for e$^+$e$^-\rightarrow$ HZ, proportional to $\cos^2(\beta-\alpha)$, is large.
- The *gluophobic* scenario is constructed such that the Higgs coupling to gluons is suppressed due to a cancellation between the top and the stop loops at the hgg vertex. Since at the LHC the seraches will rely heavily on producing the Higgs boson by gluon-gluon fusion, such a scenario may be difficult to study at the LHC. The parameters are: M_{SUSY} =

350 GeV, $M_2 = 300$ GeV, $\mu = 300$ GeV, $X_t = -750$ GeV, $m_{\tilde{g}} = 500$ Gev; $\tan\beta$ is scanned between 0.4 and 40 and m_A from zero to 1 TeV.

- In the *small* α_{eff} scenario the couplings governing the decays $\mathrm{h}\rightarrow\mathrm{b\bar{b}}$ and $\mathrm{h}\rightarrow\tau^+\tau^-$ are suppressed with respect to their Standard Model values by a factor $-\sin\alpha_\mathrm{eff}/\cos\beta$ due to $\tilde{\mathrm{b}} - \tilde{g}$ loops. The suppression occurs mainly for large $\tan\beta$ and moderate m_A. The parameters are: $M_{SUSY} = 800$ GeV, $M_2 = 500$ GeV, $\mu = 2$ TeV, $X_t = -1100$ GeV, $m_{\tilde{g}} = 500$ Gev; $\tan\beta$ is scanned between 0.4 and 40 and m_A from zero to 1 TeV.

2.2 The CP-violating scenario

In the CP-violating MSSM scenario the three neutral Higgs eigenstates H_i $(i = 1,2,3)$ do not have well defined CP quantum numbers. Each of them can thus be produced by Higgsstrahlung ($\mathrm{e^+e^-}\rightarrow \mathrm{H}_i\mathrm{Z}$) via the CP-even field component, and also in pairs ($\mathrm{e^+e^-}\rightarrow \mathrm{H}_i\mathrm{H}_j$ $(i \neq j)$), the relative rates depending on the CP-even/odd mixing.

Experimentally, the CP-violating scenario is more challenging than the CP-conserving scenario. For a wide range of model parameters the lightest Higgs boson H_1 may decouple almost entirely from the Z boson. Furthermore, the second- and third-lightest H_2 and H_3 bosons may both have masses beyond the kinematic reach of LEP. One therefore anticipates a reduced search sensitivity for the CP-violating scenario.

The cross sections for Higgsstrahlung and pair production are given by [9]

$$\sigma_{\mathrm{H}_i\mathrm{Z}} = g^2_{\mathrm{H}_i\mathrm{ZZ}}\ \sigma^{SM}_{\mathrm{HZ}} \tag{5}$$

$$\sigma_{\mathrm{H}_i\mathrm{H}_j} = g^2_{\mathrm{H}_i\mathrm{H}_j\mathrm{Z}}\ \bar{\lambda}\ \sigma^{SM}_{\mathrm{HZ}} \tag{6}$$

(in the expression of $\bar{\lambda}$, Eq. (3), the indices h and A have to be replaced by H_i and H_j). The couplings

$$g_{\mathrm{H}_i\mathrm{ZZ}} = \cos\beta\mathcal{O}_{1i} + \sin\beta\mathcal{O}_{2i} \tag{7}$$

$$g_{\mathrm{H}_i\mathrm{H}_j\mathrm{Z}} = \mathcal{O}_{3i}(\cos\beta\mathcal{O}_{2j} - \sin\beta\mathcal{O}_{1j}) - \mathcal{O}_{3j}(\cos\beta\mathcal{O}_{2i} - \sin\beta\mathcal{O}_{1i}) \tag{8}$$

obey the sum rules

$$\sum_{i=1}^{3} g^2_{\mathrm{H}_i\mathrm{ZZ}} = 1 \tag{9}$$

$$g_{\mathrm{H}_k\mathrm{ZZ}} = \sum_{i,j=1}^{3} \varepsilon_{ijk} g_{\mathrm{H}_i\mathrm{H}_j\mathrm{Z}} \tag{10}$$

where ε_{ijk} is the usual Levi-Civita symbol.

The orthogonal matrix $\mathcal{O}_{ij}$ $(i,j = 1,2,3)$ relating the weak CP eigenstates to the mass eigenstates has non-zero off-diagonal elements,

$$\mathcal{O}^2_{ij} \propto \frac{m_t^4}{v^2}\frac{\mathrm{Im}(\mu A)}{32\pi^2 M^2_{\mathrm{SUSY}}}, \tag{11}$$

with $v = \sqrt{v_1^2 + v_2^2}$. Their size is a measure of the effects from CP violation in the Higgs sector. Large deviations from the CP-conserving scenario are thus expected for small $M_{\rm SUSY}$ and large $\mathrm{Im}(\mu A)$, which is obtained if the CP-violating phase, $\arg A$, takes the value 90°. Furthermore, the effects from CP violation strongly depend on the precise value of the top quark mass, which is known with a large experimental error [14].

Regarding the decay properties, the CP-violating scenario maintains a certain similarity to the CP-conserving scenario. The lightest mass eigenstate H_1 predominantly decays to $\mathrm{b\bar{b}}$ if kinematically allowed, with a small fraction decaying to $\tau^+\tau^-$ and $\mathrm{c\bar{c}}$. The second-lightest Higgs boson H_2 may decay to $\mathrm{H}_1\mathrm{H}_1$ when kinematically allowed; otherwise it decays preferentially to $\mathrm{b\bar{b}}$.

2.3 CP-violating MSSM "benchmark" models

The parameters of the benchmark model *CPX* have been chosen [17] to maximise the phenomenological differences with respect to the CP-conserving scenario. In the choice of the parameter values one also had to take into account some constraints from measurements of the electron and neutron electric dipole moments [18]. The basic set of parameters are listed in the last column of Table 1.

This scenario is examined using the two theoretical approaches incorporated in the FeynHiggs 2.0 code and in the CPH code. The following parameters have been vaied one-by-one while the other parameters have been kept at their *CPX* value.

- Top quark mass: $m_\mathrm{t} = 169.3, 174.3,\ 179.3$ and 183.0 GeV/c^2, embracing the current experimental value, $m_\mathrm{t} = 178.0 \pm\ 4.3$ GeV/c^2 [14].
- The CP-violating phase: $\arg(A_{\mathrm{t,b}}) = 0°,\ 30°,\ 60°,\ 90°$ (CPX value), 135° and 180° (the values 0° and 180° correspond to CP-conserving limits).
- The Higgs mass parameter: $\mu = 0.5$ (CPX value), $1.0, 2.0$ and 4.0 TeV.
- The SUSY breaking scale: $M_{SUSY} = 0.5$ TeV (CPX value) and 1.0 TeV. The proposal of the CPX scenario [17] predicts a weak dependence on M_{SUSY} if the relations $|A_{\mathrm{t,b}}| = |m_{\tilde{g}}| = \mu/2 = 2M_{SUSY}$ are preserved. This behaviour is examined by studying also a model with $M_{SUSY} = 1$ TeV and the values of $A_{\mathrm{t,b}},\ m_{\tilde{g}}$ and μ fixed by these relation.

3 Experimental searches

The searches carried out by the four LEP collaborations are based on $\mathrm{e^+e^-}$ collision data which span a large range of centre-of-mass energies, from 91 GeV to 209 GeV. The searches include the Higgsstrahlung process and pair production processes, ensuring by their complementarity a high sensitivity over the accessible MSSM parameter space. It is important to note that the kinematic properties of the signal processes are to a large extent independent of the CP composition of the Higgs bosons. This implies that the same topological searches can be applied to study the CP-conserving and CP-violating scenarios. For Higgsstrahlung this is natural since only the CP-even components of the Higgs fields couple to the Z boson. In pair production involving CP-even and CP-odd field components (which may even oscillate), the similarity of the kinematic properties (e.g., angular distributions) results from the scalar nature of the Higgs bosons. Small differences may occur from spin-spin correlations between final-state particles but these do not give noticeable differences in the signal detection efficiencies. We therefore adopt a common notation for the CP-conserving and CP-violating processes where $\mathcal{H}_i$ $(i = 1, 2, 3)$ designates three generic neutral Higgs bosons with undefined CP properties which, in the CP-conserving limit ($\arg A = 0°$) become the CP eigenstates h, A and H.

For each of the four experiments, the data analysis is done in several steps. A preselection is applied to reduce some of the largest backgrounds, in particular, from two-photon processes. The remaining background, mainly from fermion pairs and WW or ZZ production, (possibly accompanied by photon or gluon radiation) is further reduced by more selective cuts or by applying multivariate techniques such as likelihood analyses and neural networks. The identification of b-quarks in the decay of the Higgs bosons plays an important role in the discrimination between signal and background, as does the kinematic reconstruction of the Higgs boson mass. The detailed implementation of these analyses, as well as the data samples used by the four collaborations, is described in the individual publications [10–13]. A full catalog of the searches provided by the four LEP collaborations for this combination, with corresponding references to the detailed descriptions, are listed in the Appendix.

3.1 Search topologies

Searches have been carried out for the two main signal processes, the Higgsstrahlung process $e^+e^- \to \mathcal{H}_1 Z$ and the pair production process $e^+e^- \to \mathcal{H}_2\mathcal{H}_1$.

(A) Considering first the Higsstrahlung process $e^+e^- \to \mathcal{H}_1 Z$, the principal signal topologies are those used in the search for the Standard Model Higgs boson [3], namely

- the four-jet topology $e^+e^- \to (\mathcal{H} \to b\bar{b})(Z \to q\bar{q})$ where the invariant mass of two jets is close to the Z boson mass m_Z while the other two jets contain b-flavour;
- the missing energy topology $e^+e^- \to (\mathcal{H} \to b\bar{b}, \tau^+\tau^-)(Z \to \nu\bar{\nu})$ where the event consists of two b-jets and substantial missing momentum and missing mass, compatible with m_Z;
- the leptonic final states, $e^+e^- \to (\mathcal{H} \to b\bar{b}, q\bar{q})(Z \to e^+e^-, \mu^+\mu^-)$, where the invariant mass of the two leptons is close to m_Z;
- the final states with tau-leptons, $e^+e^- \to (\mathcal{H} \to \tau^+\tau^-)(Z \to q\bar{q})$ and $(\mathcal{H} \to b\bar{b}, \tau^+\tau^-)(Z \to \tau^+\tau^-)$, where either the $\tau^+\tau^-$ or the $q\bar{q}$ pair has an invariant mass close to m_Z.

Most of these signatures are relevant for Higgs boson masses above the $b\bar{b}$ threshold and rely on the identification of b-quarks in the final state. Ssearches for lighter Higgs bosons were using other signatures; they are also listed in the Appendix. In some regions of the MSSM parameter space, however, the $\mathcal{H}_1 \to b\bar{b}$ channel may be suppressed and decays into other quark flavours or gluon pairs are favoured. The above searches are therefore complemented and replaced, whenever more efficient, by

- flavour-independent searches for $e^+e^- \to (\mathcal{H}_1 \to q\bar{q})Z$ which do not explicitly require b-flavour.
- Finally, the searches for Higgsstrahlung also include the Higgs cascade decay $e^+e^- \to (\mathcal{H}_2 \to \mathcal{H}_1\ \mathcal{H}_1)Z$, giving rise to a new class of event topologies. These may play an important role in regions of the parameter space where they are allowed by kinematics.

(B) In the case of the pair production process $e^+e^- \to \mathcal{H}_2\mathcal{H}_1$, the principal signal topologies are

- the four-b final state $(\mathcal{H}_2 \to b\bar{b})(\mathcal{H}_1 \to b\bar{b})$,
- the mixed final states $(\mathcal{H}_2 \to \tau^+\tau^-)(\mathcal{H}_1 \to b\bar{b})$ and $(\mathcal{H}_2 \to b\bar{b})(\mathcal{H}_1 \to \tau^+\tau^-)$,
- the four-tau final state $(\mathcal{H}_2 \to \tau^+\tau^-)(\mathcal{H}_1 \to \tau^+\tau^-)$
- and the Higgs cascade decay $(\mathcal{H}_2 \to \mathcal{H}_1\mathcal{H}_1)\mathcal{H}_1$, giving rise to event topologies banging between six b-jets and six tau-leptons.

The above searches are relevant to Higgs boson masses above the $\tau^+\tau^-$ threshold (other signatures are used for lighter Higgs bosons). These searches are also supplemented and replaced, whenever more efficient, by

- flavour-independent searches for $e^+e^- \to \mathcal{H}_2\mathcal{H}_1$ where the b-flavour of the jets is not explicitly required.

3.2 Additional experimental constraints

If the combination of the above searches is not sufficiently sensitive for excluding a given model point, the following additional constraints are applied.

- Constraint from the measured decay width of the Z boson, Γ_Z, and its possible deviation $\Delta\Gamma_Z$ from the Standard Model prediction. The model point is regarded as excluded if the following relation between the cross sections is found to be true:

$$\sum_i \sigma_{\mathcal{H}_i Z}(m_Z) + \sum_{i,j} \sigma_{\mathcal{H}_i\mathcal{H}_j}(m_Z) > \frac{\Delta\Gamma_Z}{\Gamma_Z} \cdot \sigma_Z^{tot}(m_Z). \quad (12)$$

Here $\Delta\Gamma_Z = 6.5$ MeV is taken from [22] and σ_Z^{tot} is the Z pole cross section calculated using the program ZFITTER [23].

- Constraints from decay mode independent search for $e^+e^- \to \mathcal{H}_1 Z$ [24]. The model point is regarded as excluded if the condition

$$\sigma_{\mathcal{H}_i Z}(m_{\mathcal{H}_i}) > k(m_{\mathcal{H}_i}) \cdot \sigma_{HZ}^{SM}(m_{\mathcal{H}_i}) \tag{13}$$

  is fulfilled, where $k(m_{\mathcal{H}_i})$ is the scale factor applied to the Standard Model Higgs cross section that is excluded at 95% c.l. .

- Constraints from a search for light Higgs boson produced by the Yukawa process [25]. The model point is regarded as excluded if the predicted Yukawa enhancement factor $\xi(m_{\mathcal{H}_1})$ is excluded by this search.

These additional constraints are particularly efficient at small $m_{\mathcal{H}_i}$ below the $b\bar{b}$ threshold.

3.3 Statistical combination of search channels

The statistical method by which the topological searches are combined is described in Refs. [3, 26].

After selection, the combined data configuration (distribution of all selected events in several discriminating variables) is compared in a frequentist approach to a large number of simulated configurations generated separately for two hypotheses: the background (b) hypothesis and the signal plus background ($s+b$) hypothesis. The ratio

$$Q = \mathcal{L}_{s+b}/\mathcal{L}_b \tag{14}$$

of the corresponding likelihoods is used as the test statistic. The predicted, normalised, distributions of Q (probability density functions) are integrated to obtain the p-values [27] $1 - CL_b = 1 - \mathcal{P}_b(Q \le Q_{observed})$ and $CL_{s+b} = \mathcal{P}_{s+b}(Q \le Q_{observed})$; these measure the compatibility of the observed data configuration with the two hypotheses.

Systematic errors are incorporated in the calculation of confidences by randomly varying the signal and background estimates in each channel[1]. For a given source of uncertainty, correlations are addressed by applying these random variations simultaneously to all those channels where the uncertainty is relevant. Errors which are correlated between the experiments arise mainly from using the same Monte Carlo generators and cross section calculations, for example, for the signal processes. The uncorrelated errors are dominated by the limited statistics of the simulated background event samples.

[1]The word "channel" designates any subset of the data where a search has been carried out. These subsets may correspond to specific final-state topologies, to data sets collected at different centre-of-mass energies or to the subsets of data collected by different experiments.

The frequentist exclusion limit is usually computed from the confidence CL_{s+b} for the signal plus background hypothesis: a signal is regarded as excluded at the 95% c.l. if an observation is made such that CL_{s+b} is lower than 0.05. However, this procedure may lead to the undesired situation where a large downward fluctuation of the background would exclude a signal hypothesis for which the experiment has no sensitivity since the expected signal rate is too small. This problem is avoided by using the ratio

$$CL_s = CL_{s+b}/CL_b \tag{15}$$

instead of CL_{s+b}. We adopt this quantity for setting exclusion limits and consider a given model to be excluded at the 95% c.l. if the corresponding value of CL_s is less than 0.05. Since CL_b is a positive number less than one, CL_s will always be greater than CL_{s+b} and the limit obtained will therefore be conservative.

4 Limits on topological cross sections

In this section we present upper bounds on cross sections for the most important final-state topologies expected from the Higgsstrahlung process $e^+e^- \rightarrow \mathcal{H}_1 Z$ and the pair production process $e^+e^- \rightarrow \mathcal{H}_2\mathcal{H}_1$. We define a scaling factor

$$S_{95} = \sigma_{max}/\sigma_{ref} \tag{16}$$

where σ_{max} is the largest cross section compatible with the data at the 95% c.l. and σ_{ref} is a reference cross section. For the final-state topologies motivated by the Higgsstrahlung process, σ_{ref} is taken to be the Standard Model Higgs production cross section; therefore, in models with two Higgs field doublets, the limit on S_{95} can be interpreted as a limit $\sin^2(\beta - \alpha)$ (see Eq. (1)). For the final-state topologies motivated by the pair-production process, σ_{ref} is taken to be the MSSM Higgs production cross section of Eq. (2) with $\cos^2(\beta - \alpha)$=1.

Figure 1 shows S_{95} for final states motivated by the Higgsstrahlung process $e^+e^- \rightarrow \mathcal{H}_1 Z$. In part (a) the Higgs boson is assumed to decay into fermions and bosons with branching ratios according to the Standard Model. Contributions from the fusion processes WW$\rightarrow$ H and ZZ$\rightarrow$ H are are included; they are assumed to scale like those from the Higgsstrahlung process. In parts (b) it is assumed that the Higgs boson decays exclusively to $b\bar{b}$ and in part (c) to $\tau^+\tau^-$ pairs. Besides representing model independent bounds, this figure also illustrates the overall agreement between the data and the expected background from Standard Model processes. The largest deviations observed barely exceed two standard deviations.

Figure 2 shows contours of S_{95} for the Higgsstrahlung cascade process $e^+e^- \rightarrow (\mathcal{H}_2 \rightarrow \mathcal{H}_1\mathcal{H}_1)Z$, projected onto the ($\mathcal{H}_2$, $\mathcal{H}_1$) plane, assuming that the $\mathcal{H}_2$ boson decays exclusively to $\mathcal{H}_1\mathcal{H}_1$. In part (a) it is assumed that $\mathcal{H}_1$ decays exclusively into $b\bar{b}$ and in part (b) to $\tau^+\tau^-$. In part (c) an equal mixture of $\mathcal{H}_1 \rightarrow b\bar{b}$ and $\mathcal{H}_1 \rightarrow \tau^+\tau^-$ is assumed, which implies a mixture of 25% $b\bar{b}b\bar{b}Z$, 25% $\tau^+\tau^-\tau^+\tau^-Z$ and 50% $b\bar{b}\tau^+\tau^-Z$ final states.

Figure 3 shows S_{95} for final states motivated by the pair-production process $e^+e^- \rightarrow \mathcal{H}_2\mathcal{H}_1$, for the particular case where the masses $m_{\mathcal{H}_2}$ and $m_{\mathcal{H}_1}$ are approximately equal. Such is the case, for example, in the CP-conserving MSSM scenarios for $\tan\beta$ larger than about 10. The abscissa represents the sum $m_{\mathcal{H}_2}+ m_{\mathcal{H}_1}$. In part (a) of the figure the $\mathcal{H}_2$ and $\mathcal{H}_1$ decay branching ratios correspond to the m_h-*max* benchmark scenario with $\tan\beta$= 10 (see the caption for the exact values). In part (b) both $\mathcal{H}_2$ and $\mathcal{H}_1$ are assumed to decay exclusively to $\mathrm{b\bar{b}}$ and in part (c) to $\tau^+\tau^-$. In part (d) one Higgs boson is assumed to decay exclusively to $\mathrm{b\bar{b}}$ while the other exclusively to $\tau^+\tau^-$. Besides representing model independent bounds, this figure also illustrates the overall agreement between the data and the expected background from Standard Model processes. The largest deviations observed are within two standard deviations.

Figure 4 shows contours of S_{95} for final states motivated by the process $\mathrm{e^+e^-}\rightarrow\mathcal{H}_2\mathcal{H}_1$, projected onto the ($\mathcal{H}_1$, $\mathcal{H}_2$) plane.

Figure 5 shows contours of S_{95} for the pair-production cascade decay $\mathrm{e^+e^-}\rightarrow(\mathcal{H}_2\rightarrow\mathcal{H}_1\mathcal{H}_1)\mathcal{H}_1$, projected onto the ($\mathcal{H}_1$, $\mathcal{H}_2$) plane, assuming that the $\mathcal{H}_2$ boson decays exclusively to $\mathcal{H}_1\mathcal{H}_1$. In part (a) $\mathcal{H}_1$ decays exclusively to $\mathrm{b\bar{b}}$ and in part (b) to $\tau^+\tau^-$. In part (c) an equal mixture of $\mathcal{H}_1\rightarrow\mathrm{b\bar{b}}$ and $\mathcal{H}_1\rightarrow\tau^+\tau^-$ is assumed, which implies 12.5% $\mathrm{b\bar{b}b\bar{b}b\bar{b}}$, 37.5% $\mathrm{b\bar{b}b\bar{b}}\tau^+\tau^-$, 37.5% $\mathrm{bb}\tau^+\tau^-\tau^+\tau^-$ and 12.5% $\tau^+\tau^-\tau^+\tau^-\tau^+\tau^-$ final states.

5 Results interpreted in the CP-conserving MSSM scenario

The agreement of the data with the expectation based on Monte Carlo simulation, with no signal, is illustrated in Figure 6. The figure is based on the observed p-values $1 - CL_b$ and is meant to show the statistical significances of possible signal-like excesses in the data. While the situation with background only corresponds to p-values close to 0.5, a signal-like excess would result in much smaller values. For example, an excess of three (five) standard deviations would give rise to a p-value of 2.7 10^{-3} (5.7 10^{-7}). This test is made using predictions of the CP-conserving MSSM benchmark scenario m_h-max.

Over the bulk part of the parameter space the local excesses are smaller than two standard deviations. The lowest p-value, in the region of m_h around 100 GeV, has a p-value of 5 10^{-3}, corresponding to 2.8 standard deviations. This excess stems for the Higgsstrahlung search and is discussed in Ref. [3] in the context of the search for the Standard Model Higgs boson.

The 95% c.l. exclusions for the CP-conserving benchmark scenario m_h-*max* are shown in Figure 7 in four projections of the parameter space, and compared to the exclusions expected on the basis of Monte Carlo simulations with no signal. The theoretical limits of the MSSM parameter space are indicated. For $\tan\beta$ less than about five the exclusion is mainly provided by the Higgsstrahlung process, resulting in lower bounds of about 114 GeV/c^2 for m_h. For higher values of $\tan\beta$ the exclusion is provided mainly by the pair-production processes, with limits in the vicinity of 93 GeV/c^2 for both m_h and m_A. The precise mass limits for this and the other CP-conserving scenarios are liste in Table 2.

The data also exclude a certain domain of $\tan\beta$, as illustrated in plots (b), (c) and (d). The exclusion is best visible in the projection (m_{h}, $\tan\beta$) (see plot (b)) which also shows its dependence on the precise value of the top quark mass. The excluded values of $\tan\beta$ are summarised in Table 3. For m_{t} =183.0 GeV/c^2, no limit can be set in this scenario. One should note, however, that the mass bounds listed in Table 2 are largely insensitive to m_{t}.

Figures 8 and 9 show the same set of plots for the two variants of the m_{h}-*max* scenario introduced in Section 2.1.2. (See Table 2 for the corresponding limits.) (*** Discussion ***)

The 95% c.l. exclusions for the CP-conserving benchmark scenario with *no mixing* is shown in Figure 10. While the experimental exclusions are very similar, the theoretical bounds of the parameter space are more restricted than in the m_{h}-*max* scenario. The precise limits are listed in Tables 2 and 3.

Attention should be drawn to a small domain at $m_{\mathrm{h}}\approx$80 GeV/c^2, small m_{A} and $\tan\beta$<0.7, which is not excluded in this scenario. In this domain the branching ratio for $\mathrm{h}\rightarrow\mathrm{b\bar{b}}$ is small and the decay of the A boson, with mass below the $\tau^+\tau^-$ threshold, is model dependent. For this reason, the mass limits listed in Tables 2 and 3 for this scenario are strictly valid only for $\tan\beta\geq$0.7.

Figure 11 shows the exclusion plots for the variant of the *no-mix* scenario introduced in Section 2.1.2. (See Table 2 for the corresponding limits.) (*** Discussion ***)

The 95% c.l. exclusions for the *large-μ* benchmark scenario are shown in Figure 12. As mentioned in Subsection 2.3, this scenario was constructed to test the sensitivity of LEP to MSSM scenarios which are a priori difficult to tackle experimentally since the Higgs boson decays to $\mathrm{b\bar{b}}$ are largely suppressed. It turns out that the LEP searches, in particular the flavour-independent ones, are sufficiently powerful to exclude almost all such situations. There remains one thin unexcluded strips at large m_{A} and large $\tan\beta$. Here the values of CL_s scatter between 0.06 and 0.11, in agreement with the CL_s values expected from Monte Carlo simulation with no signal, and the values of $1-CL_b$ are between 0.37 and 0.65. Thus, this strip is at the edge of being excluded at the 95% c.l. . (See Table 2 for the corresponding limits.)

Similar plots are shown in Figures 13 and 14 for the *gluophobic* and *small-α_{eff}* scenarios defined in Section 2.1.3. (See Table 2 for the corresponding limits.) (*** Discussion ***)

6 Results interpreted in the CP-violating MSSM scenario

The agreement of the data with the expectation based on Monte Carlo simulation, with no signal, is illustrated in Figure 15. The test is made for the CP-violating MSSM benchmark scenario *CPH*. Over the largest part of the parameter space the local excesses are smaller than two standard deviations. The lowest p-value, in the region of m_{h} around 100 GeV (?), has a p-value of 5 10^{-3} (?), corresponding to 2.8 (?) standard deviations (this excess, in the Higgsstrahlung channel, was discussed in the context of the search for the Standard Model Higgs boson [3]). The experimental exclusions for the CP-violating *CPX* benchmark scenario (see Table 1 for the parameters) are shown in Figure 16. The top mass is fixed at 179.3 GeV/c^2. The exclusions are presented in four projections. The theoretical limits of the MSSM parameter space are indicated and the experimental exclusions are compared, at the 95% c.l., to the exclusions expected on the basis of Monte Carlo simulations with no signal. The dark-gray (dark-green) regions are excluded at the 99.7% c.l. For large $m_{\mathcal{H}_2}$, the $\mathcal{H}_1$ is almost completely CP-even. In this case the exclusion limit is close to the one obtained for the Standard Model Higgs boson [3]. For example, for $m_{\mathcal{H}_2}$ larger than 130 GeV/c^2, one can cite a lower bound of 113 GeV/c^2 (?) for the lightest neutral Higgs boson $\mathcal{H}_1$. Large CP-odd admixtures to $\mathcal{H}_1$ occur for $m_{\mathcal{H}_2}$ lower than 130 GeV/c^2, giving rise to unexcluded domains. The exclusion completely disappears for $\tan\beta$ between about 4 and 10. In this region the sharing of the signal between the Higgsstrahlung processes $e^+e^-\rightarrow\mathcal{H}_1Z$ and $\mathcal{H}_2Z$ and, at $\tan\beta$ close to 10, also with $e^+e^-\rightarrow H_1H_2$, causes an overall loss of the search sensitivity. Nonetheless, the region defined by $m_{\mathcal{H}_1}<$ 114 GeV/c^2 and $\tan\beta<$ 3.5 (?) is excluded by the data (see part (b) of the figure). Furthermore, a general 95% c.l. lower bound of $\tan\beta>$ 2.8 (?) can be set in the *CPX* scenario (see parts (c) and (d) of the figure).

As already mentioned in Subsection 2.3, the two theoretical approaches, CPH and FeynHiggs 2.0, give slightly different exclusions. The plots in Figure 16 were thus obtained by chosing in each point of the parameter space the more conservative of the two approaches (less significant exclusion). The results using either one or the other calculation are shown, for the $(m_{\mathcal{H}_1}, \tan\beta)$ projection, in Figure 17. The largest difference occurs at large $\tan\beta$ where the FeynHiggs calculation predicts a larger Higgsstrahlung cross-section and hence a better search sensitivity than the CPH calculation.

The large impact of the top mass, which could be anticipated from Eq. (11), is illustrated in Figure 18 where the $(m_{h_1}, \tan\beta)$ projection is shown for four values of m_t, comprising the current experimental value and its error [14]. One observes a strong reduction of the exclusion power as one increases m_t from 169.3 GeV/c^2 to 183.0 GeV/c^2, especially in the region of $\tan\beta$ between 4 and 10. Lower bounds on the Higgs boson masses cannot be quoted due to the lack of exclusion in this domain. Note that the p-value $1-CL_b$ is greater than 5 10^{-3}(?) everywhere, even for the highest value of the top mass; hence the lack of exclusion is not generated by an excess in the data but rather by a loss of search sensitivity. Note that the lower bound on $\tan\beta$ quoted above is barely sensitive to the precise value of the top quark mass; for m_t = 183.0 GeV/c^2 it is still $\tan\beta>$ 2.5 (?).

Figure 19 illustrates the exclusion in the $(m_{\mathcal{H}_1},\ \tan\beta)$ plane as a function of the CP-violating phase, arg A. For phase angles close to 0° the parameter space and the experimental exclusions are similar to those in the CP-conserving scenarios (see, for example, Fig. **??**). Siseable modifications are observed for larger phase angles, especially for $\arg A = 90°$ (the *CPX* value). As the phase angle increases further, one approaches gradually again the CP-conserving scenario. At $\arg A = 180°$ the theoretically allowed parameter space is appears to be divided in two domains, which are almost completely excluded by the searches. In the region separating the two domains (between $\tan\beta$ of about 12 and 32), the theoretical calculations become uncertain (*** some explanation is needed here ***). Hence, no exclusion can be claimed in this domain.

In Figure 20 the value of the Higgs mass parameter μ is varied from 500 GeV through 2000 GeV (the *CPX* value) to 4000 GeV. At low values the CP-violating effects are small (see Eq. 6) and the exclusion power is strong as in the CP-conserving case. For values much larger than $\mu = 2000$ GeV (the *CPX* value), the calculation following CPH becomes uncertain at large $\tan\beta$. In this region, the predictions of both the FeynHiggs and the CPH calculations are uncertain because the bottom-Yukawa coupling becomes non-perturbative. This results in negative values for the square of some Higgs masses and other unphysical results. Hence, no exclusion can be claimed in this domain.

It is interesting to note that for $\mu = 4000$ GeV (see plot (d)) the region with $m_{\mathcal{H}_1}$ larger than 60 GeV/c^2 and $\tan\beta$ larger than 10 is largely excluded while it is not for the *CPX* value $\mu = 2000$ GeV (see plot (c)). This difference is traced to a delicate balance between the predicted cross-sections for $\mathcal{H}_1$Z and $\mathcal{H}_2\mathcal{H}_1$. For $\mu = 4000$ GeV the $\mathcal{H}_1$Z cross-section increases in that region and the combined LEP data are sufficient to exclude the model via the Higgsstrahlung process.

Figure 21 illustrates the dependence on the soft SUSY breaking scale parameter m_{SUSY}, the value of which is increased from 500 GeV (the *CPX* value) to 1000 GeV. This increase decreases the CP-violating effects (see Eq. 6) and hence lead to a better exclusion. The relative insensitivity to changes of m_{SUSY} while preserving the relations $|A_{\mathrm{t,b}}| = |m_{\tilde{g}}| = \mu/2 = 2M_{SUSY}$, mentioned in Section 2.3, is qualitatively confirmed by comparing plot (c) to plots (a) and (b).

7 Summary

The searches for neutral Higgs bosons described in this paper are based on data collected by the four LEP collaborations, ALEPH, DELPHI, L3 and OPAL. The data samples include those collected during the LEP 2 phase at energies up to 209 GeV and, for two experiments, also the LEP 1 data collected at energies in the vicinity of the Z boson resonance. The searches address a large number of final-state topologies resulting from the Higgsstrahlung process $\mathrm{e}^+\mathrm{e}^-\rightarrow\mathcal{H}\mathrm{Z}$ and from the pair production process $\mathrm{e}^+\mathrm{e}^-\rightarrow\mathcal{H}_1\mathcal{H}_2$. All these searches are statistically combined. The combined LEP data do not reveal any significant excess of events which would indicate a signal for the production of Higgs bosons. The differences with respect to the background prediction are typically below two standard deviations, with a few exceptions where they are between two and three standard deviations.

From these results, upper bounds are derived for the cross section of a number of Higgs-like event topologies. These upper bounds cover a wide range of Higgs boson masses and are typically much lower than the largest cross sections predicted within the MSSM framework for the same event topology.

The combined search results are used to test a largenumber of MSSM scenarios which include CP-conserving and CP-violating benchmark models. It is found that in all these scenarios the searches conducted at LEP exclude sizeable domains of the theoretically allowed parameter space. In the CP-violating scenarios studied the excluded lomains are smalled than in the CP-conserving scenarios.

In some cases, lower bounds can be set on the masses of neutral Higgs bosons and the value of $\tan\beta$ can also be restricted. For example, taking the CP-conserving model m_{h}-*max*, values of m_{h} and m_{A} less than 92.9(?) GeV/c^2 and 93.4(?) GeV/c^2, respectively, are excluded as well as values of $\tan\beta$ between 0.9(?) and 1.5(?) for $m_{\mathrm{t}} = 179.3$ GeV/c^2. For lower values of m_{t} the excluded range of $\tan\beta$ is larger, for higher m_{t} it is more narrow. In the CP-violating benchmark scenario *CPX* the combined LEP data show large unexcluded domains down to the smallest masses; hence, no absolute limits can be set for the Higgs boson masses. On the other hand, $\tan\beta$ can be restricted to values larger than 2.6 for $m_{\mathrm{t}} = 179.3$ GeV/c^2. This bound is rather insensitive to the precise choice ot the top quark mass.

Acknowledgements

We congratulate the LEP Accelerator Division for the successful running of LEP during twelve years, up to the highest energies. We also would like to express our thanks to the engineers and technicians in all our institutions for their contributions to the excellent performance of the four LEP experiments. The LEP Working Group for Higgs Boson Searches acknowledges the fruitful cooperation between the experiments in exchanging their experimental results and developing and applying the procedures for the statistical combination.

References

[1] P.W. Higgs, Phys. Lett. **12** (1964) 132;
idem, Phys. Rev. Lett. **13** (1964) 508;
idem, Phys. Rev. **145** (1966) 1156;
F. Englert and R. Brout, Phys. Rev. Lett. **13** (1964) 321;
G.S. Guralnik, C.R. Hagen and T.W.B. Kibble, Phys. Rev. Lett. **13** (1964) 585.

[2] S. Weinberg, Phys. Rev. Lett. **19** (1967) 1264;
A. Salam, *Elementary Particle Theory*, ed. N. Svartholm (Almquist and Wiksells, Stockholm, 1968), 367.

[3] ALEPH, DELPHI, L3 and OPAL Collaborations, The LEP working group for Higgs boson searches, Phys. Lett. **B565** (2003) 61.

[4] J. Wess and B. Zumino, Nucl. Phys. **B70** (1974) 39;
idem, Phys. Lett. **49B** (1974) 52;
P. Fayet, Phys. Lett. **69B** (1977) 489;
ibid. **84B** (1979) 421, *ibid.* **86B** (1979) 272.

[5] W. de Boer and Ch. Sander, Phys. Lett. **B585** (2004) 276.

[6] H.E. Haber and G.L. Kane, Phys. Rep. **C117** (1985) 75;
J.F. Gunion, H.E. Haber, G.L. Kane and S. Dawson, *The Higgs Hunter's Guide* (Addison-Wesley) 1990;
H.E. Haber, *Supersymmetry*, Phys. Rev. **D66** (2002) 010001-895.

[7] Y. Okada, M. Yamaguchi and T. Yanagida, Theor. Phys **85** (1991)1;
H. Haber and R. Hempfling, Phys. Rev. Lett. **66** (1991) 1815;
J. Ellis, G. Ridolfi and F. Zwirner, Phys. Lett. **B257** (1991) 83;
R. Barbieri and M. Frigeni, Phys. Lett. **B258** (1991) 395;
M. Carena, M. Quiros and C.E.M. Wagner, Nucl. Phys. **B461** (1996) 407;
H. Haber, R. Hempfling and A. Hoang, Z. Phys. **C75** (1997) 539;
S. Heinemeyer, W. Hollik and G. Weiglein, Eur. Phys. Jour. **C9** (1999) 343;
S. Heinemeyer, W. Hollik and G. Weiglein, Phys. Rev. **D58** (1998) 091701, Phys. Lett. **B440** (1998) 296, hep-ph/9807423 and JHEP 0006 (2000) 009;
J. R. Espinosa and R.-J. Zhang, Nucl. Phys. **B586** (2000) 3;
A. Brignole, G. Degrassi, P. Slavich and F. Zwirner, Nucl. Phys. **B631** (2002) 195;
G. Degrassi, S. Heinemeyer, W. Hollik, P. Slavich and G. Weiglein, Eur. Phys. J. **C28** (2003) 133.

[8] A. D. Sakharov, JETP Lett. **5** (1967) 24;
M. Carena et al., Nucl. Phys. **B599** (2001) 158.

[9] A. Pilaftsis,*Phys. Rev.* **D 58** (1998) 096010;
idem, *Phys. Lett.* **B 435** (1998) 88.
D. Demir, *Phys. Rev.* **D 60** (1999) 055006;

S. Choi, M. Drees and J. Lee, *Phys. Lett.* **B 481** (2000) 57;
A. Pilaftsis and C. Wagner, *Nucl. Phys.* **B 553** (1999) 3, hep-ph/9902371;
M. Carena, J. Ellis, A. Pilaftsis and C. Wagner, *Nucl. Phys.* **B 586** (2000) 92;
T. Ibrahim and P. Nath, *Phys. Rev.* **D 63** (2001) 035009;
Phys. Rev. **D 66** (2002) 015005;
S. Heinemeyer, *Eur. Phys. Jour.* **C 22** (2001) 521;
M. Frank, S. Heinemeyer, W. Hollik and G. Weiglein, *Supersymmetry and unification of fundamental interactions*, hep-ph/0212037, Proceedings, SUSY02, DESY, Hamburg (Germany), July 2002, vol.2, p.637.

[10] OPAL Collab. G. Abbiendi et al., Eur. Phys. J. **C37** (2004) 49.

[11] ALEPH Collab., A. Heister et al., Phys. Lett. **B 526** (2002) 191.

[12] DELPHI Collab., J. Abdallah et al., Eur. Phys. J. **C32** (2004) 145.

[13] L3 Collab., P. Achard et al., Phys. Lett. **B 545** (2002) 30.

[14] The CDF and D0 Collaborations and the Tevatron Electroweak Working Group, TEVEWWWG/top 2004/01, hep-ex/0404010 (2004).

[15] S. Heinemeyer and W. Hollik, Nucl. Phys. **B474** (1996) 32.

[16] M. Carena, S. Heinemeyer, C.E.M. Wagner and G. Weiglein, hep-ph/9912223;
idem, Eur. Phys. Journ. **C26** (2003) 601.

[17] M. Carena, J. R. Ellis, A. Pilaftsis and C. E. Wagner, Phys. Lett. B **495** (2000) 155;
idem, Nucl. Phys. **B586** (2000) 92.

[18] E. D. Commins, S. B. Ross, D. DeMille and B. C. Regan, Phys. Rev. A **50** (1994) 2960;
P. G. Harris *et al.*, Phys. Rev. Lett. **82** (1999) 904.

[19] S. Heinemeyer, W. Hollik and G. Weiglein, *Comp. Phys. Comm.* **124** 2000 76;
M. Frank, S. Heinemeyer, W. Hollik and G. Weiglein, hep-ph/0212037.
The code is accessible via `http://www.feynhiggs.de` .

[20] M. Carena, M. Quirós and C.E.M. Wagner, Nucl. Phys. **B461** (1996) 407;
M. Carena, S. Mrenna and C. Wagner, Phys. Rev. D60 (1999) 075010;
M. Carena, H. E. Haber, S. Heinemeyer, W. Hollik, C. E. M. Wagner and G. Weiglein, Nucl. Phys. **B580** (2000) 29;
J. R. Espinosa and R.-J. Zhang, JHEP 0003 (2000) 026.

[21] P. Janot, *Physics at LEP2*, Ed. G. Altarelli, T. Sjöstrand and F. Zwirner, CERN 96-01 Vol. 2, p. 309.

[22] The LEP Collaborations ALEPH, DELPHI, L3, OPAL, the LEP Electroweak Working Group, and the SLD Heavy Flavour and Electroweak Groups, arXiv:hep-ex/0212036.

[23] D. Y. Bardin, P. Christova, M. Jack, L. Kalinovskaya, A. Olchevski, S. Riemann and T. Riemann, Comp. Phys. Comm. **133** (2001) 229.

[24] OPAL Collab., G. Abbiendi *et al.*, Eur. Phys. J **C 27** (2003) 311.

[25] OPAL Collab., G. Abbiendi *et al.*, Eur. Phys. J. C **23** (2002) 397.

[26] T. Junk, Nucl. Instr. Meth. Phys. Res. **A434** (1999) 435;
A. Read, in *1st Workshop on Confidence Limits*, CERN-2000-005;
P. Bock, *Computation of confidence levels for exclusion or discovery of a signal with the method of fractional event counting*, hep-ex/0405072 (2004).

[27] K. Hagiwara et al., Phys. Rev. D66, 010001-1 (2002), Review No. 31 on *Statistics*, p. 229.

[28] ALEPH Collab., D. Buskulic et al., Phys. Lett. **B 313** (1993) 549;
DELPHI Collab., P. Abreu et al., Nucl. Phys. **B 342** (1990) 1;
idem,Z. Phys. **C 51** (1991) 25;
L3 Collab., M. Acciarri et al., Phys. Lett. **B 385** (1996) 454;
OPAL Collab., P.D. Acton etal., Phys. Lett. **B 268** (1991) 122.

[29] G. W. Bennett *et al.*, Phys. Rev. Lett. **89** (2002) 101804;
Erratum: ibid. **89** (2002) 129903.

[30] Experimental results on BR(b$\rightarrow$ sγ).

[31] The ALEPH Collaboration, Eur. Phys. J. **C17** (2000) 223.

[32] The ALEPH Collaboration, Phys. Lett. **B499** (2001) 53.

[33] The ALEPH Collaboration, Phys. Lett. **B495** (2000) 1.

[34] The ALEPH Collaboration, Phys. Lett. **B526** (2002) 191.

[35] The ALEPH Collaboration, Phys. Lett. **B544** (2002) 25.

[36] DELPHI Collaboration, P. Abreu et al., Z. Phys. **C51** (1991) 25

[37] DELPHI Collaboration, P. Abreu et al., Nucl. Phys. **B342** (1990) 1

[38] DELPHI Collaboration, P. Abreu et al., Nucl. Phys. **B373** (1992) 3

[39] DELPHI Collaboration, P. Abreu et al., Nucl. Phys. **B421** (1994) 3

[40] DELPHI Collaboration, P. Abreu et al., Eur. Phys. J. **C2** (1998) 1.

[41] DELPHI Collaboration, P. Abreu et al., Eur. Phys. J. **C10** (1999) 563.

[42] DELPHI Collaboration, P. Abreu et al., Eur. Phys. J. **C17** (2000) 187, addendum Eur. Phys. J. **C17** (2000) 529.

[43] DELPHI Collaboration, J. Abdallah et al., Eur. Phys. J. **C32** (2004) 145.

[44] DELPHI Collaboration, J. Abdallah et al., CERN-EP-PH/2004-066.

[45] DELPHI Collaboration, J. Abdallah et al., Eur. Phys. J. **C23** (2002) 409.

[46] DELPHI 92-80 Dallas PHYS 191, *Neutral Higgs Bosons in a Two Doublet Model*, contribution to the 1992 ICHEP conference; quoted by G.Wormser, in proc. of the XXVI ICHEP conference (Dallas, August 1992), Vol. 2, pages 1309-14, ref. 4.

[47] DELPHI 2003-045-CONF-665, *DELPHI results on neutral Higgs bosons in MSSM benchmark scenarios*, contribution to the 2003 summer conferences.

[48] S. Dagoret, PhD Thesis, Université de Paris-Sud, Centre d'Orsay, LAL-preprint 91-12 (May 1991).

[49] DELPHI Collaboration, P. Abreu et al., Phys. Lett **B245** (1990) 276.

[50] DELPHI Collaboration, J. Abdallah et al., Eur. Phys. J. **C38** (2004) 1.

[51] DELPHI Collaboration, P. Abreu et al., Z. Phys. **C67** (1995) 69.

[52] The L3 Collaboration, M. Acciarri *et al.*, Phys. Lett. **B461** (1999) 376.

[53] The L3 Collaboration, M. Acciarri *et al.*, Phys. Lett. **B508** (2001) 225.

[54] The L3 Collaboration, P. Achard *et al.*, Phys. Lett. **B517** (2001) 319.

[55] The L3 Collaboration, P. Achard *et al.*, Phys. Lett. **B583** (2004) 14.

[56] The L3 Collaboration, P. Achard *et al.*, Phys. Lett. **B545** (2002) 30.

[57] The L3 Collaboration, M. Acciarri *et al.*, Phys. Lett. **B471** (1999) 321.

[58] The L3 Collaboration, M. Acciarri *et al.*, Phys. Lett. **B503** (2001) 21.

[59] The OPAL Collaboration, G. Alexander *et. al.*, Z. Phys. **C73** (1997) 189.

[60] The OPAL Collaboration, R. Akers *et. al.*, Z. Phys. **C64** (1994) 1.

[61] The OPAL Collaboration, K. Ackerstaff *et. al.*, Eur. Phys. J. **C1** (1998) 425.

[62] The OPAL Collaboration, K. Ackerstaff *et. al.*, Eur. Phys. J. **C5** (1998) 19.

[63] The OPAL Collaboration, G. Abbiendi *et. al.*, Eur. Phys. J. **C7** (1999) 407.

[64] The OPAL Collaboration, G. Abbiendi *et. al.*, Eur. Phys. J. **C12** (2000) 567.

[65] The OPAL Collaboration, G.Abbiendi *et al.*, Eur. Phys. J. **C26** (2003) 479.

[66] The OPAL Collaboration, G. Abbiendi *et. al.*, Eur. Phys. J. **C18** (2001) 425.

[67] The OPAL Collaboration, G. Abbiendi *et al.*, Eur. Phys. J. **C40** (2005) 317

[68] The OPAL Collaboration, G.Abbiendi *et al.*, Eur. Phys. J. **C27** (2003) 483.

Benchmark scenario		m_{h} (GeV/c^2)	m_{A} (GeV/c^2)	$\tan\beta$
m_{h}-max	observed	92.9	93.4	$0.9 < \tan\beta < 1.5$
	expected	94.8	95.1	$0.8 < \tan\beta < 1.6$
(a)	observed			
	expected			
(b)	observed			
	expected			
no-mixing ,	observed	93.3	93.3	$0.4 < \tan\beta < 5.6$
	expected	95.0	95.0	$0.4 < \tan\beta < 6.5$
(a)	observed			
	expected			
large-μ ,	observed			
	expected			
gluophobic ,	observed			
	expected			
large-α_{eff} ,	observed			
	expected			

Table 2: *Lower mass bounds and exclusions in* $\tan\beta$*, at 95% c.l., for the CP-conserving MSSM benchmark scenarios. In each case, the numbers in the first line represent the observed limits and those in the second line the median expected limits based on Monte Carlo simulations with no signal. The exclusions in* $\tan\beta$ *depend critically on the top quark mass; they are given here for* $m_{\mathrm{t}} = 179.3$ GeV/c^2.

Benchmark scenario	m_{h} (GeV/c^2)	m_{A} (GeV/c^2)	$\tan\beta$
m_{h}-max , m_{t}=169.3 GeV/c^2 m_{t}=174.3 GeV/c^2 m_{t}=179.3 GeV/c^2 m_{t}=183.0 GeV/c^2	92.9	93.4	$0.9 < \tan\beta < 1.5$
no-mixing , m_{t}=169.3 GeV/c^2 m_{t}=174.3 GeV/c^2 m_{t}=179.3 GeV/c^2 m_{t}=183.0 GeV/c^2	92.9	93.4	$0.9 < \tan\beta < 1.5$

Table 3: *The observed lower mass bounds and exclusions in* $\tan\beta$*, at 95% c.l., for the CP-conserving MSSM benchmark scenarios* m_{h}*-max and no-mixing, for various values of the top quark mass.*

8 Appendix: Catalog of searches

The searches of the four LEP collaborations which contribute to the present, combined analysis are listed in Tables 4 to 11. The list is structured in two tables per experiment, one for the Higgsstrahlung channel, $e^+e^- \rightarrow \mathcal{H}_1 Z$, and one for the pair production process, $e^+e^- \rightarrow \mathcal{H}_2\mathcal{H}_1$. In each of these tables, where it applies, the upper part contains the final states of the direct process and the lower part those of the cascade process with $\mathcal{H}_2 \rightarrow \mathcal{H}_1\mathcal{H}_1$.

The final-state topologies are listed in the first column. In the notation adopted, $\mathcal{H}_1$ represents the lightest and $\mathcal{H}_2$ the second-lightest neutral Higgs boson. In the CP-conserving case, $\mathcal{H}_1$ is identified with the CP-even eigenstate h. The assignement of $\mathcal{H}_2$ is not quite obvious. Typically, it is identified with the CP-odd eigenstate A˜ (the cascade process $\mathcal{H}_2 \rightarrow \mathcal{H}_1\mathcal{H}_1$ can be identified with h→ AA); however, in exceptional cases, $\mathcal{H}_2$ may also designate the heavier CP-even Higgs boson ∵

The symbol q indicates any of the quark flavour, s, u, d, s, c or b, unspecified. "Hadrons" also include gluons. In the missing energy channel, in addition to the $\mathcal{H}_1 Z \rightarrow \mathcal{H}_1 \nu\bar{\nu}$ process, the W fusion process $\mathcal{H}_1 \nu_e \bar{\nu}_e$ (including interference) is also considered in the calculation of the cross-section; similarly, in the leptonic channel, in addition to the $\mathcal{H}_1 Z \rightarrow \mathcal{H}_1 \ell^+\ell^-$ process, the Z fusion process $\mathcal{H}_1 e^+e^-$ (including interference) is also considered.

The contributions based on LEP1 data can be identified by their value "91" in the column listing the e^+e^- collision energy $\sqrt{s}$ (GeV); they represent an integrated luminosity $\mathcal{L}$ of about 125 pb^{-1}. The LEP2 data span over a large range of e^+e^- energies between 133 GeV and 209 GeV; they represent an integrated luminosity of about 2400 pb^{-1}. With increasing data samples and e^+e^- energies, the sensitivity was extended to increasingly high Higgs boson masses. Thus, the searches were regularly updated or replaced by new analyses, more efficient at the higher masses. The Higgs boson mass ranges where the individual searches are relevant are listed in the tables. In the last column, a reference is given to the publications where the details of the individual searches are described.

	$\sqrt{s}$ (GeV)	$\mathcal{L}$ (pb^{-1})	Mass range (GeV/c^2)	Ref.
$\mathcal{H}_1$Z$\rightarrow$ (...) (...)			$m_{\mathcal{H}1}$	
$(\mathrm{b\bar{b}})(\mathrm{q\bar{q}})$	189	176.2	75 – 110	[31]
$(\mathrm{b\bar{b}}, \mathrm{c\bar{c}}, \tau\tau, \mathrm{gg})(\nu\bar{\nu})$	189	176.2	75 – 110	[31]
$(\mathcal{H}_1)(\mathrm{e^+e^-},\ \mu^+\mu^-)$	189		75 – 110	[31]
$(\mathrm{b\bar{b}})(\tau^+\tau^-), (\tau^+\tau^-)(\mathrm{q\bar{q}})$	189	176.2	65 – 110	[31]
$(\mathrm{b\bar{b}})(\mathrm{q\bar{q}})$	192 – 202	236.7	60 – 120	[32]
$(\mathrm{b\bar{b}})(\nu\bar{\nu})$	192 – 202	236.7	60 – 120	[32]
$(\mathrm{b\bar{b}}, \tau^+\tau^-, (\mathrm{c\bar{c}} + \mathrm{gg}))(\mathrm{e^+e^-}, \mu^+\mu^-)$	192 – 202	236.7	60 – 120	[32]
$(\mathrm{b\bar{b}}, \tau^+\tau^-, \mathrm{c\bar{c}}, \mathrm{gg})(\tau^+\tau^-), (\tau^+\tau^-)(\mathrm{q\bar{q}})$	192 – 202	236.7	60 – 120	[32]
$(\mathrm{b\bar{b}})(\mathrm{q\bar{q}})$	199 – 209	217.2	75 – 120	[33, 34]
$(\mathrm{b\bar{b}}, \tau^+\tau^-, \mathrm{c\bar{c}}, \mathrm{gg}, \mathrm{WW})(\nu\bar{\nu})$	199 – 209	217.2	75 – 120	[33, 34]
$(\mathrm{b\bar{b}}, \tau^+\tau^-, (\mathrm{c\bar{c}} + \mathrm{gg}))(\mathrm{e^+e^-}, \mu^+\mu^-)$	199 – 209	217.2	70 – 130	[33, 34]
$(\mathrm{b\bar{b}}, \tau^+\tau^-, \mathrm{c\bar{c}}, \mathrm{gg}, \mathrm{WW})(\tau^+\tau^-)$	199 – 209	217.2	75 – 120	[33, 34]
$(\tau^+\tau^-)(\mathrm{q\bar{q}})$	199 – 209	217.2	75 – 120	[33, 34]
$(\mathrm{b\bar{b}} + \mathrm{c\bar{c}} + \mathrm{s\bar{s}} + \mathrm{gg})(\mathrm{q\bar{q}})$	189	176.2	40 – 100	[35]
$(\mathrm{b\bar{b}} + \mathrm{c\bar{c}} + \mathrm{s\bar{s}} + \mathrm{gg})(\nu\bar{\nu})$	189	176.2	60 – 100	[35]
$(\mathrm{b\bar{b}} + \mathrm{c\bar{c}} + \mathrm{s\bar{s}} + \mathrm{gg})(\mathrm{e^+e^-}, \mu^+\mu^-)$	189	176.2	60 – 115	[31, 35]
$(\mathrm{b\bar{b}} + \mathrm{c\bar{c}} + \mathrm{s\bar{s}} + \mathrm{gg})(\mathrm{q\bar{q}})$	192 – 202	236.7	40 – 110	[35]
$(\mathrm{b\bar{b}} + \mathrm{c\bar{c}} + \mathrm{s\bar{s}} + \mathrm{gg})(\nu\bar{\nu})$	192 – 202	236.7	60 – 116	[35]
$(\mathrm{b\bar{b}} + \mathrm{c\bar{c}} + \mathrm{s\bar{s}} + \mathrm{gg})(\mathrm{e^+e^-}, \mu^+\mu^-)$	192 – 202	236.7	60 – 115	[32, 35]
$(\mathrm{b\bar{b}} + \mathrm{c\bar{c}} + \mathrm{s\bar{s}} + \mathrm{gg})(\mathrm{q\bar{q}})$	199 – 209	217.2	40 – 115	[35]
$(\mathrm{b\bar{b}} + \mathrm{c\bar{c}} + \mathrm{s\bar{s}} + \mathrm{gg})(\nu\bar{\nu})$	199 – 209	217.2	75 – 120	[35]
$(\mathrm{b\bar{b}} + \mathrm{c\bar{c}} + \mathrm{s\bar{s}} + \mathrm{gg})(\mathrm{e^+e^-}, \mu^+\mu^-)$	199 – 209	217.2	70 – 130	[33–35]

Table 4: *Summary of the ALEPH searches for the Higgsstrahlung process* $\mathrm{e^+e^-}\rightarrow\mathcal{H}_1\mathrm{Z}$*, originally developed for the search for the SM Higgs boson. In the leptonic channel, the event selection for the SM Higgs boson searches is used, and the signal efficiency has been evaluated for the indicated hadronic decays of the Higgs boson. In the* $(\tau^+\tau^-)(\mathrm{q\bar{q}})$ *the SM Higgs boson search is used.*

	$\sqrt{s}$ (GeV)	$\mathcal{L}$ (pb^{-1})	Mass range (GeV/c^2)	Ref.
$\mathcal{H}_2\mathcal{H}_1\rightarrow$ (...)(...)			$(m_{\mathcal{H}_2}+m_{\mathcal{H}_1})/2$	
(bb)(bb)	189	176.2	65 – 95	[31]
$(\tau^+\tau^-)(\mathrm{b\bar{b}}), (\mathrm{b\bar{b}})(\tau^+\tau^-)$	189	176.2	65 – 95	[31]
$(\mathrm{b\bar{b}})(\mathrm{b\bar{b}})$	192 – 202	236.7	$60 - \sqrt{s}/2$	[32]
$(\mathrm{b\bar{b}}, \tau^+\tau^-, \mathrm{c\bar{c}}, \mathrm{gg})(\tau^+\tau^-)$	192 – 202	236.7	$60 - \sqrt{s}/2$	[32]
$(\tau^+\tau^-)(\mathrm{b\bar{b}}, \tau^+\tau^-, \mathrm{c\bar{c}}, \mathrm{gg})$	192 – 202	236.7	$60 - \sqrt{s}/2$	[32]
$(\mathrm{b\bar{b}})(\mathrm{b\bar{b}})$	199 – 209	217.2	$75 - \sqrt{s}/2$	[33, 34]
$(\mathrm{b\bar{b}}, \tau^+\tau^-, \mathrm{c\bar{c}}, \mathrm{gg})(\tau^+\tau^-)$	199 – 209	217.2	$75 - \sqrt{s}/2$	[33, 34]
$(\tau^+\tau^-)(\mathrm{b\bar{b}}, \tau^+\tau^-, \mathrm{c\bar{c}}, \mathrm{gg})$	199 – 209	217.2	$75 - \sqrt{s}/2$	[33, 34]

Table 5: *Summary of the ALEPH searches for the pair production process* $\mathrm{e^+e^-}\rightarrow \mathcal{H}_2\mathcal{H}_1$. *The searches are restricted to* $|m_{\mathcal{H}_2}$-$m_{\mathcal{H}_1}|$ *less than about 20* GeV/c^2.

	$\sqrt{s}$ (GeV)	$\mathcal{L}$ (pb^{-1})	Mass ranges (GeV/c^2)		Ref.
$e^+e^-\to\mathcal{H}_1Z\to(...)(...)$			$m_{\mathcal{H}_1}$		
$Z\to e^+e^-$, $\mu^+\mu^-$	91	2.5	< 0.21		[36]
(V^0)(any)	91	2.5	< 0.21		[36]
(2 prongs)($q\bar{q}$)	91	0.5	$0.21 - 2$		[37]
(jet)(e^+e^-, $\mu^+\mu^-$)	91	0.5	$1 - 20$		[37]
(jet jet)($Z\ell^+\ell^-$, $\nu\bar{\nu}$)	91	3.6	$12 - 50$		[38]
(jet jet)(e^+e^-, $\mu^+\mu^-$, $\nu\bar{\nu}$)	91	33.4	$35 - 70$		[39]
($b\bar{b}$)(any), ($\tau^+\tau^-$)($q\bar{q}$)	161,172	19.9	$40 - 80$		[40]
($b\bar{b}$)(any), ($\tau^+\tau^-$)($q\bar{q}$)	183	52.0	$45 - 95$		[41]
($b\bar{b}$)(any), ($\tau^+\tau^-$)(qq)	189	158.0	$65 - 100$		[42]
($b\bar{b}$)(any)	192-208	452.4	$12 - 120$		[43,45]
($\tau^+\tau^-$)(qq)	192-208	452.4	$45 - 120$		[43,45]
($q\bar{q}$, gg)($q\bar{q}$, $\nu\bar{\nu}$, e^+e^-, $\mu^+\mu^-$)	189-208	610.4	$4 - 116$		[44]
$e^+e^-\to\mathcal{H}_1Z\to(\mathcal{H}_1\mathcal{H}_1)Z\to(...)(...)$			$m_{\mathcal{H}_2}$	$m_{\mathcal{H}_1}$	
$Z\to q\bar{q}$	91	16.2	$12 - 70$	< 0.21	[46]
(V^0V^0)(any but $\tau^+\tau^-$)	91	9.7	$0.5 - 55$	< 0.21	[46]
($\gamma\gamma$)(any)	91	12.5	$0.5 - 60$	< 0.21	[46]
(4 prongs)(any)	91	12.9	$0.5 - 60$	$0.21 - 10$	[46]
(hadrons) ($\nu\bar{\nu}$)	91	15.1	$1 - 60$	$0.21 - 30$	[46]
($\tau^+\tau^-\tau^+\tau^-$)($\nu\bar{\nu}$)	91	15.1	$9 - 60$	$3.5 - 12$	[46]
(any)($q\bar{q}$, $\nu\bar{\nu}$)	161,172	20.0	$40 - 70$	$20 - 35$	[40]
($b\bar{b}b\bar{b}$) ($q\bar{q}$)	183	54.0	$45 - 85$	$12 - 40$	[41]
($b\bar{b}b\bar{b}$, $b\bar{b}c\bar{c}$, $c\bar{c}c\bar{c}$)($q\bar{q}$)	192-208	452.4	$30 - 105$	$12 - 50$	[43,45]
($c\bar{c}c\bar{c}$)($q\bar{q}$)	192-208	452.4	$10 - 105$	$4 - 12$	[47]

Table 6: *List of the DELPHI searches for the Higgsstrahlung process* $e^+e^-\to\mathcal{H}_1Z$.

	$\sqrt{s}$ (GeV)	$\mathcal{L}$ (pb^{-1})	Mass ranges (GeV/c^2)		Ref.
$e^+e^- \to \mathcal{H}_2\mathcal{H}_1 \to (...)(...)$			$m_{\mathcal{H}_2}$	$m_{\mathcal{H}_1}$	
4 prongs	91	5.3	$0.2-10$	$0.2-10$	[39]
$\tau^+\tau^-$ hadrons	91	0.5	$4-35$	$4-35$	[48]
$\tau^+\tau^-$ jet jet	91	3.6	$25-42$	$25-42$	[49]
$b\bar{b}b\bar{b}$, $b\bar{b}c\bar{c}$	91	33.4	$15-46$	$15-46$	[38]
$\tau^+\tau^- b\bar{b}$	91	79.4	$4-70$	$4-70$	[47]
$b\bar{b}b\bar{b}$	91	79.4	$12-40$	$20-70$	[50]
$b\bar{b}b\bar{b}$	133	6.0	$40-68$	$35-73$	[51]
$b\bar{b}b\bar{b}$, $\tau^+\tau^- b\bar{b}$	161,172	20.0	$40-70$	$35-75$	[40]
$b\bar{b}b\bar{b}$, $\tau^+\tau^- b\bar{b}$	183	54.0	$50-80$	$25-105$	[41]
$b\bar{b}b\bar{b}$, $\tau^+\tau^- b\bar{b}$	189	158.0	$65-90$	$40-115$	[42]
$\tau^+\tau^- b\bar{b}$	192-208	452.4	$50-100$	$60-150$	[43, 45]
$b\bar{b}b\bar{b}$	192-208	452.4	$12-100$	$40-190$	[43, 45]
$\tau^+\tau^-\tau^+\tau^-$	189-208	570.9	$4-90$	$4-170$	[50]
$b\bar{b}b\bar{b}$	189-208	610.2	$12-70$	$30-170$	[50]
quarks or gluons	189-208	610.4	$4-170$	$4-170$	[44]
$e^+e^- \to \mathcal{H}_2\mathcal{H}_1 \to (\mathcal{H}_1\mathcal{H}_1)\mathcal{H}_1 \to (...)(...)$			$m_{\mathcal{H}_2}$	$m_{\mathcal{H}_1}$	
$(\gamma\gamma)(\gamma\gamma)$	91	12.5	$0.5-60$	< 0.21	[46]
(4 prongs)(2 prongs)	91	12.9	$0.5-60$	$0.21-10$	[46]
(hadrons)(hadrons)	91	15.1	$1-60$	$0.21-30$	[46]
$(\tau^+\tau^-\tau^+\tau^-)(\tau^+\tau^-)$	91	15.1	$9-60$	$3.5-12$	[46]
(any)(any)	161,172	20.0	$40-70$	$20-35$	[40]

Table 7: *List of the DELPHI searches for pair production* $e^+e^- \to \mathcal{H}_2\mathcal{H}_1$.

	$\sqrt{s}$ (GeV)	$\mathcal{L}$ (pb^{-1})	Mass ranges (GeV/c^2)		Ref.
$e^+e^-\to\mathcal{H}_1 Z\to$ (...)(...)			$m_{\mathcal{H}_1}$		
(bb)(any)	189	176.4	60 – 100		[52]
$(\tau^+\tau^-)(q\bar{q})$	189	176.4	60 – 100		[52]
$(b\bar{b})$(any)	192 – 202	233.2	60 – 110		[53]
$(\tau^+\tau^-)(q\bar{q})$	192 – 202	233.2	60 – 110		[53]
$(b\bar{b})$(any)	203 – 209	217.3	60 – 120		[54]
$(\tau^+\tau^-)(q\bar{q})$	203 – 209	217.3	60 – 120		[54]
$(b\bar{b}, c\bar{c}, gg)$(any)	189	176.4	60 – 100		[55]
$(b\bar{b}, c\bar{c}, gg)$(any)	192 – 202	233.2	60 – 110		[55]
$(b\bar{b}, c\bar{c}, gg)$(any)	204 – 209	214.5	60 – 120		[55]
$e^+e^-\to\mathcal{H}_2 Z\to(\mathcal{H}_1\mathcal{H}_1)Z\to$ (...)(...)			$m_{\mathcal{H}_2}$	$m_{\mathcal{H}_1}$	
$(\mathcal{H}_1\to bb, c\bar{c}, gg)(q\bar{q})$	189 – 209	626.9	30 – 85	10 – 42	[56]

Table 8: *List of the L3 searches for the Higgsstrahlung processes* $e^+e^-\to\mathcal{H}_1 Z$.

	$\sqrt{s}$ (GeV)	$\mathcal{L}$ (pb^{-1})	Mass ranges (GeV/c^2)		Ref.
$e^+e^-\to\mathcal{H}_2\mathcal{H}_1\to$ (...)(...)			$m_{\mathcal{H}_2}$	$m_{\mathcal{H}_1}$	
$(b\bar{b})(b\bar{b})$, $(b\bar{b})(\tau^+\tau^-)$, $(\tau^+\tau^-)(b\bar{b})$	189	176.4	50 – 95	50 – 95	[57]
$(b\bar{b})(b\bar{b})$, $(b\bar{b})(\tau^+\tau^-)$, $(\tau^+\tau^-)(b\bar{b})$	192 – 202	233.2	50 – 105	50 – 105	[58]
$(b\bar{b})(b\bar{b})$, $(b\bar{b})(\tau^+\tau^-)$, $(\tau^+\tau^-)(b\bar{b})$	204 – 209	216.6	50 – 110	50 – 110	[56]

Table 9: *List of the L3 searches for the pair production process* $e^+e^-\to\mathcal{H}_2\mathcal{H}_1$.

	$\sqrt{s}$ (GeV)	$\mathcal{L}$ (pb^{-1})	Mass ranges (GeV/c^2)		Ref.
$\mathcal{H}_1$Z→ (...) (...)			$m_{\mathcal{H}_1}$		
(b$\bar{\mathrm{b}}$)(q$\bar{\mathrm{q}}$)	161–172	20.4	$40-80$		[61,62]
(b$\bar{\mathrm{b}}$)(q$\bar{\mathrm{q}}$)	183	54.1	$40-95$		[63]
(b$\bar{\mathrm{b}}$)(q$\bar{\mathrm{q}}$)	189	172.1	$40-100$		[64]
(b$\bar{\mathrm{b}}$)(q$\bar{\mathrm{q}}$)	192–209	421.2	$80-120$		[65]
(b$\bar{\mathrm{b}}$)($\nu\bar{\nu}$)	161–172	20.4	$50-70$		[61,62]
(b$\bar{\mathrm{b}}$)($\nu\bar{\nu}$)	183	53.9	$50-95$		[63]
(b$\bar{\mathrm{b}}$)($\nu\bar{\nu}$)	189	171.4	$50-100$		[64]
(b$\bar{\mathrm{b}}$)($\nu\bar{\nu}$)	192–209	419.9	$30-120$		[65]
(b$\bar{\mathrm{b}}$)($\tau^+\tau^-$), ($\tau^+\tau^-$)(q$\bar{\mathrm{q}}$)	161–172	20.4	$30-95$		[61,62]
(b$\bar{\mathrm{b}}$)($\tau^+\tau^-$), ($\tau^+\tau^-$)(q$\bar{\mathrm{q}}$)	183	53.7	$30-100$		[63]
(b$\bar{\mathrm{b}}$)($\tau^+\tau^-$), ($\tau^+\tau^-$)(q$\bar{\mathrm{q}}$)	189	168.7	$30-100$		[64]
(b$\bar{\mathrm{b}}$)($\tau^+\tau^-$), ($\tau^+\tau^-$)(q$\bar{\mathrm{q}}$)	192–209	417.4	$80-120$		[65]
(b$\bar{\mathrm{b}}$)(e$^+$e$^-$), (b$\bar{\mathrm{b}}$)($\mu^+\mu^-$)	183	55.9	$60-100$		[63]
(b$\bar{\mathrm{b}}$)(e$^+$e$^-$), (b$\bar{\mathrm{b}}$)($\mu^+\mu^-$)	189	170.0	$70-100$		[64]
(b$\bar{\mathrm{b}}$)(e$^+$e$^-$), (b$\bar{\mathrm{b}}$)($\mu^+\mu^-$)	192–209	418.3	$40-120$		[65]
(q$\bar{\mathrm{q}}$)($\tau^+\tau^-$), ($\tau^+\tau^-$)(q$\bar{\mathrm{q}}$), (q$\bar{\mathrm{q}}$)($\nu\bar{\nu}$)	91	46.3	$0-70$		[59,60]
(q$\bar{\mathrm{q}}$)(e$^+$e$^-$), (q$\bar{\mathrm{q}}$)($\mu^+\mu^-$	91	46.3	$20-70$		[59,60]
(any)(e$^+$e$^-$), (any)($\mu^+\mu^-$)	161–172	20.4	$35-80$		[61,62]
(q$\bar{\mathrm{q}}$)(q$\bar{\mathrm{q}}$)	189	174.1	$60-100$		[66]
(q$\bar{\mathrm{q}}$)(q$\bar{\mathrm{q}}$)	192–209	424.2	$60-120$		[67]
(q$\bar{\mathrm{q}}$)($\nu\bar{\nu}$)	189	171.8	$30-100$		[66]
(q$\bar{\mathrm{q}}$)($\nu\bar{\nu}$)	192–209	414.5	$30-110$		[67]
(q$\bar{\mathrm{q}}$)($\tau^+\tau^-$), ($\tau^+\tau^-$)(q$\bar{\mathrm{q}}$)	189	168.7	$30-100$		[66]
(q$\bar{\mathrm{q}}$)($\tau^+\tau^-$), ($\tau^+\tau^-$)(q$\bar{\mathrm{q}}$)	192–209	418.9	$60-115$		[67]
(q$\bar{\mathrm{q}}$)(e$^+$e$^-$), (q$\bar{\mathrm{q}}$)($\mu^+\mu^-$))	189	170.0	$70-100$		[66]
(q$\bar{\mathrm{q}}$)(e$^+$e$^-$), (q$\bar{\mathrm{q}}$)($\mu^+\mu^-$)	192–209	422.0	$60-120$		[67]
e$^+$e$^-$→$\mathcal{H}_2$Z→($\mathcal{H}_1\mathcal{H}_1$)Z→ (...)(...)			$m_{\mathcal{H}_2}$	$m_{\mathcal{H}_1}$	
(q$\bar{\mathrm{q}}$q$\bar{\mathrm{q}}$)($\nu\bar{\nu}$)	91	46.3	$10-75$	$0-35$	[59,60]
(b$\bar{\mathrm{b}}$b$\bar{\mathrm{b}}$)(q$\bar{\mathrm{q}}$)	189	172.1	$40-100$	$10.5-48$	[64]
(b$\bar{\mathrm{b}}$b$\bar{\mathrm{b}}$)(q$\bar{\mathrm{q}}$)	183	54.1	$40-80$	$10.5-38$	[63]
(b$\bar{\mathrm{b}}$b$\bar{\mathrm{b}}$)(q$\bar{\mathrm{q}}$)	192–209	421.2	$80-120$	$12-m_{\mathcal{H}}/2$	[10]
(b$\bar{\mathrm{b}}$b$\bar{\mathrm{b}}$)($\nu\bar{\nu}$)	183	53.9	$50-95$		[63]
(q$\bar{\mathrm{q}}$q$\bar{\mathrm{q}}$)($\nu\bar{\nu}$)	189	171.4	$50-100$		[64]
(b$\bar{\mathrm{b}}$b$\bar{\mathrm{b}}$)($\nu\bar{\nu}$)	199–209	207.2	$100-110$	$12-m_{\mathcal{H}}/2$	[10]
(b$\bar{\mathrm{b}}$b$\bar{\mathrm{b}}$)($\tau^+\tau^-$)	183	53.7	$30-100$		[63]
(b$\bar{\mathrm{b}}$b$\bar{\mathrm{b}}$)($\tau^+\tau^-$)	189	168.7	$30-100$		[64]
(b$\bar{\mathrm{b}}$b$\bar{\mathrm{b}}$)($\nu\bar{\nu}$, e$^+$e$^-$, $\mu^+\mu^-$)	189–192	201.7	$45-90$	$2-10.5$	[68]
(b$\bar{\mathrm{b}}$b$\bar{\mathrm{b}}$)($\nu\bar{\nu}$, e$^+$e$^-$, $\mu^+\mu^-$)	196–209	396.9	$45-90$	$2-10.5$	[68]

Table 10: *List of the OPAL searches for the Higgsstrahlung processes* e$^+$e$^-$→$\mathcal{H}_1$Z*.*

	$\sqrt{s}$ (GeV)	$\mathcal{L}$ (pb^{-1})	Mass ranges (GeV/c^2)		Ref.
$\mathcal{H}_2\mathcal{H}_1\to$(...) (...)			$m_{\mathcal{H}_2}$	$m_{\mathcal{H}_1}$	Ref.
$(b\bar{b})(b\bar{b})$	130–136	5.2	$\Sigma = 80-130$	$\Delta = 0-50$	[62]
$(b\bar{b})(b\bar{b})$	161	10.0	$\Sigma = 80-130$	$\Delta = 0-60$	[61,62]
$(b\bar{b})(b\bar{b})$	172	10.4	$\Sigma = 80-130$	$\Delta = 0-60$	[61,62]
$(b\bar{b})(b\bar{b})$	183	54.1	$\Sigma = 80-150$	$\Delta = 0-60$	[63]
$(b\bar{b})(b\bar{b})$	189	172.1	$\Sigma = 80-180$	$\Delta = 0-70$	[64]
$(b\bar{b})(b\bar{b})$	192	28.9	$\Sigma = 83-183$	$\Delta = 0-70$	[10]
$(b\bar{b})(b\bar{b})$	196	74.8	$\Sigma = 80-187$	$\Delta = 0-70$	[10]
$(b\bar{b})(b\bar{b})$	200	77.2	$\Sigma = 80-191$	$\Delta = 0-70$	[10]
$(b\bar{b})(b\bar{b})$	202	36.1	$\Sigma = 80-193$	$\Delta = 0-70$	[10]
"high $m_{\mathcal{H}_1}$" $(b\bar{b})(b\bar{b})$	199–209	207.3	$\Sigma = 120-190$	$\Delta = 0-70$	[10]
"low $m_{\mathcal{H}_1}$" $(b\bar{b})(b\bar{b})$	199–209	207.3	$\Sigma = 100-140$	$\Delta = 60-100$	[10]
$(b\bar{b})(\tau^+\tau^-)$, $(\tau^+\tau^-)(b\bar{b})$	161	10.0	$40-160$	$52-160$	[61,62]
$(b\bar{b})(\tau^+\tau^-)$, $(\tau^+\tau^-)(b\bar{b})$	172	10.4	$37-160$	$28-160$	[61,62]
$(b\bar{b})(\tau^+\tau^-)$, $(\tau^+\tau^-)(b\bar{b})$	183	53.7	$\Sigma = 70-170$	$\Delta = 0-70$	[63]
$(b\bar{b})(\tau^+\tau^-)$, $(\tau^+\tau^-)(b\bar{b})$	189	168.7	$\Sigma = 70-190$	$\Delta = 0-90$	[64]
$(b\bar{b})(\tau^+\tau^-)$, $(\tau^+\tau^-)(b\bar{b})$	192	28.7	$\Sigma = 10-174$	$\Delta = 0-182$	[10]
$(b\bar{b})(\tau^+\tau^-)$, $(\tau^+\tau^-)(b\bar{b})$	196	74.7	$\Sigma = 10-182$	$\Delta = 0-191$	[10]
$(b\bar{b})(\tau^+\tau^-)$, $(\tau^+\tau^-)(b\bar{b})$	200	74.8	$\Sigma = 10-182$	$\Delta = 0-191$	[10]
$(b\bar{b})(\tau^+\tau^-)$, $(\tau^+\tau^-)(b\bar{b})$	202	35.4	$\Sigma = 10-174$	$\Delta = 0-182$	[10]
$(b\bar{b})(\tau^+\tau^-)$, $(\tau^+\tau^-)(b\bar{b})$	199–209	203.6	$\Sigma = 70-190$	$\Delta = 0-90$	[10]
$(q\bar{q})(\tau^+\tau^-)$, $(\tau^+\tau^-)(q\bar{q})$	91	46.3	$12-75$	$10-78$	[59,60]
$e^+e^-\to\mathcal{H}_2\mathcal{H}_1\to(\mathcal{H}_1\mathcal{H}_1)\mathcal{H}_1\to$ (...)(...)			$m_{\mathcal{H}_2}$	$m_{\mathcal{H}_1}$	
$(b\bar{b}b\bar{b})(b\bar{b})$	91	27.6	$40-70$	$5-35$	[59,60]
$(b\bar{b}b\bar{b})(b\bar{b})$	130–136	5.2	$55-65$	> 27.5	[62]
$(b\bar{b}b\bar{b})(b\bar{b})$	161	10.0	$55-65$	> 20.0	[61,62]
$(b\bar{b}b\bar{b})(b\bar{b})$	172	10.4	$55-65$	$25-35$	[61,62]
$(b\bar{b}b\bar{b})(b\bar{b})$	183	54.1	$30-80$	$12-40$	[63]
$(b\bar{b}b\bar{b})(b\bar{b})$	189	172.1	$24-80$	$12-40$	[64]
$(b\bar{b}b\bar{b})(b\bar{b})$	199–209	207.3	$\Sigma = 90-200$	$\Delta = 40-160$	[10]
6τ, $4\tau 2q$, $2\tau 4q$	91	46.3	$30-75$	$4-30$	[59,60]

Table 11: *List of the OPAL searches for the pair production process* $e^+e^-\to\mathcal{H}_2\mathcal{H}_1$. *The symbols* Σ *and* Δ *stand for the mass sum* $m_{\mathcal{H}_2}+m_{\mathcal{H}_1}$ *and mass difference* $|m_{\mathcal{H}_2}-m_{\mathcal{H}_1}|$.

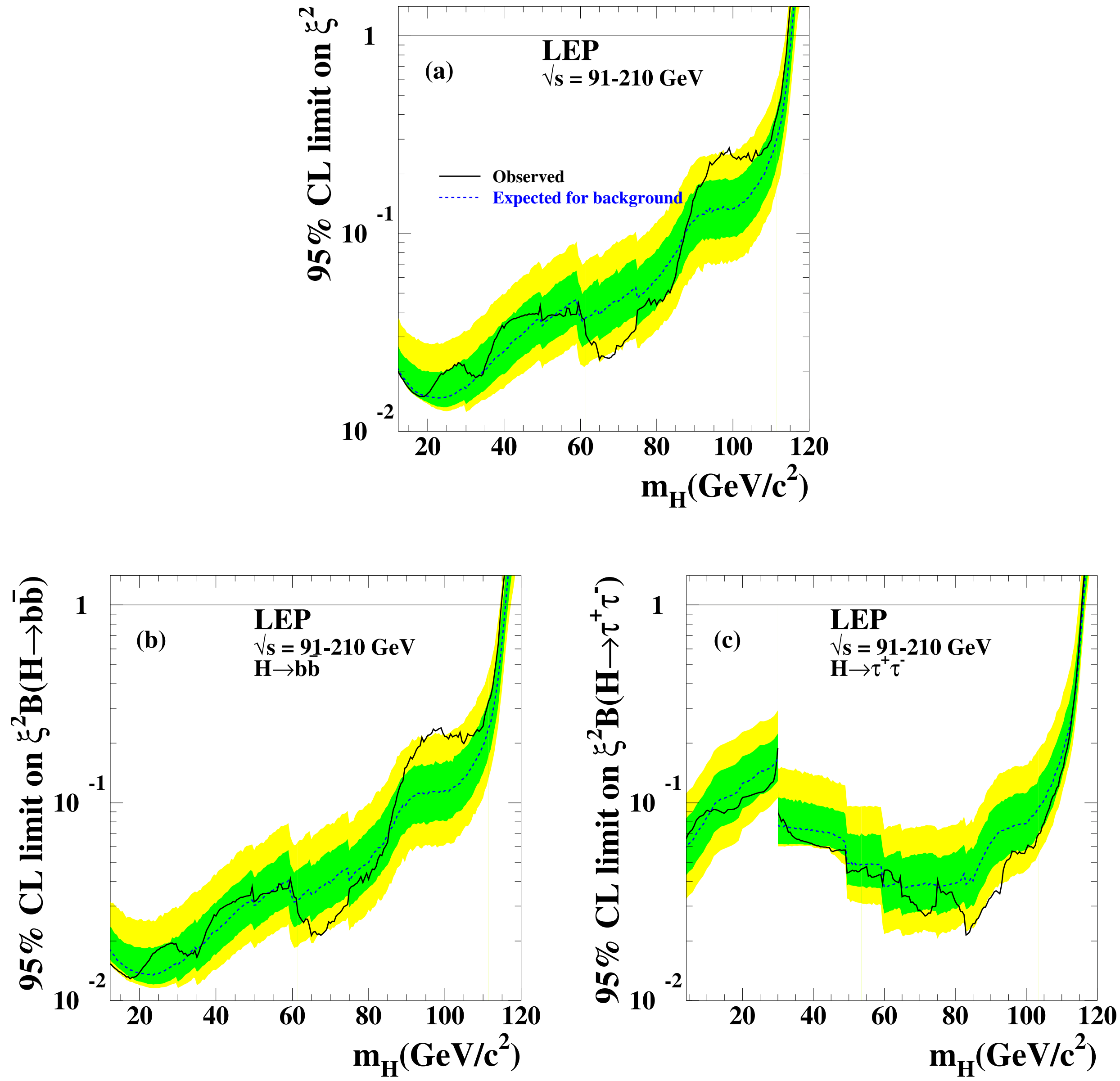

Figure 1: *Model-independent 95% c.l. upper bounds, S_{95}, for various topological cross sections motivated by the Higgsstrahlung process* $e^+e^- \rightarrow \mathcal{H}_1 Z$*, as a function of the Higgs boson mass. The full line represents the observed limit. The dark (green) and light (yellow) shaded bands around the median expectation (dashed line) correspond to the 68% and 95% probability bands. The horizontal lines correspond to the Standard Model cross section. (a) The Higgs boson decay branching ratios are assumed to be those predicted by the Standard Model; (b) the Higgs boson is assumed to decay exclusively to* $b\bar{b}$*; (c) the Higgs boson is assumed to decay exclusively to* $\tau^+\tau^-$*. (*** These figures need to be updated. Also, the denomination of the ordinates should become* S_{95} ****)*

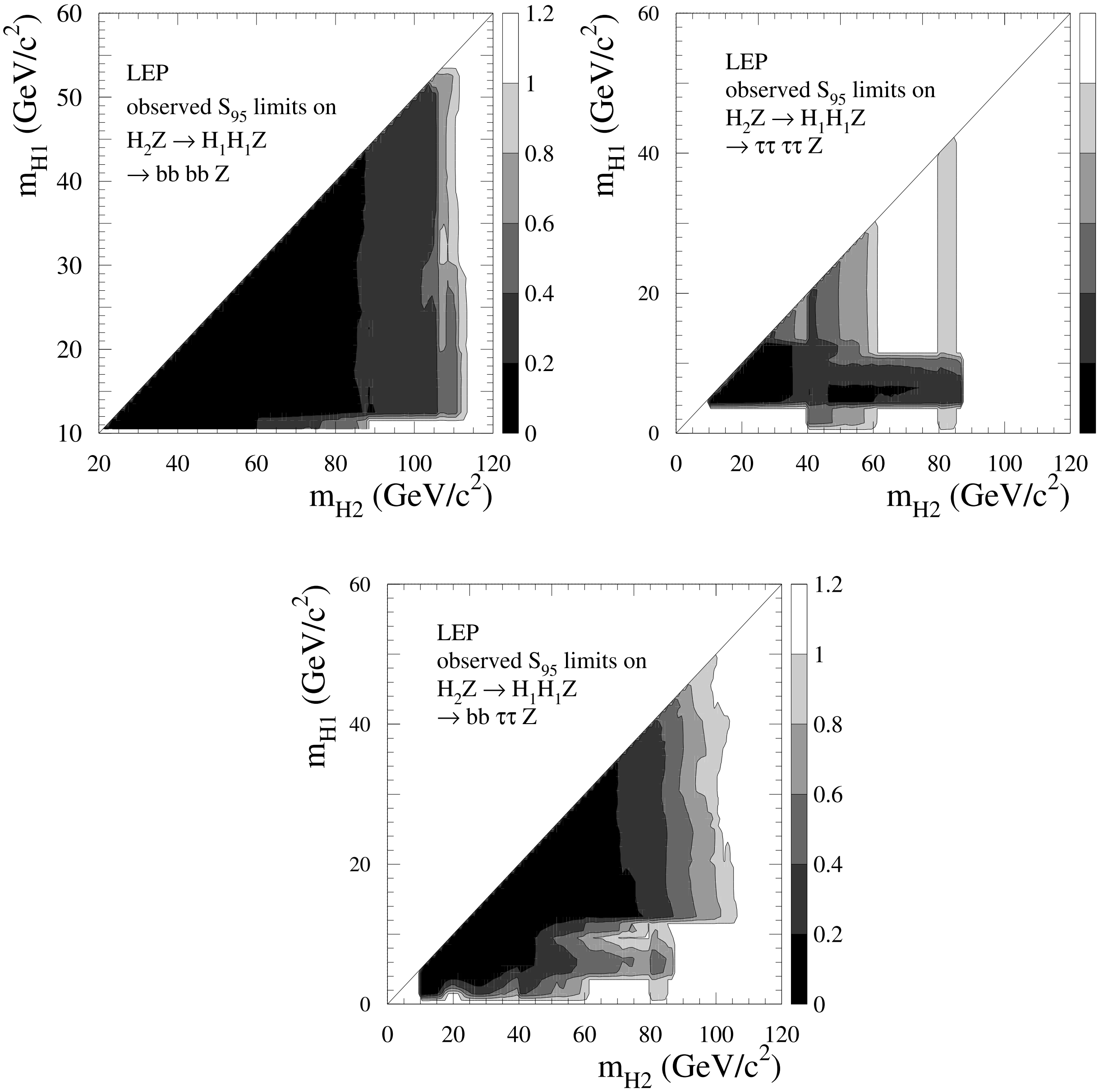

Figure 2: *Contours of the model-independent 95% c.l. upper bound, S_{95}, for various topological cross-sections motivated by the Higgsstrahlung cascade process* $e^+e^- \rightarrow (\mathcal{H}_2 \rightarrow \mathcal{H}_1\mathcal{H}_1)Z$*, projected onto the* $(m_{\mathcal{H}_2}, m_{\mathcal{H}_1})$ *plane. The scales for the shadings are given on the right-hand side of each plot. (a) The* $\mathcal{H}_1$ *boson is assumed to decay exclusively to* $b\bar{b}$*. (b) The* $\mathcal{H}_1$ *boson is assumed to decay exclusively to* $\tau^+\tau^-$*. (c) The* $\mathcal{H}_1$ *is assumed to decay with equal probability to* $b\bar{b}$ *and to* $\tau^+\tau^-$*.*

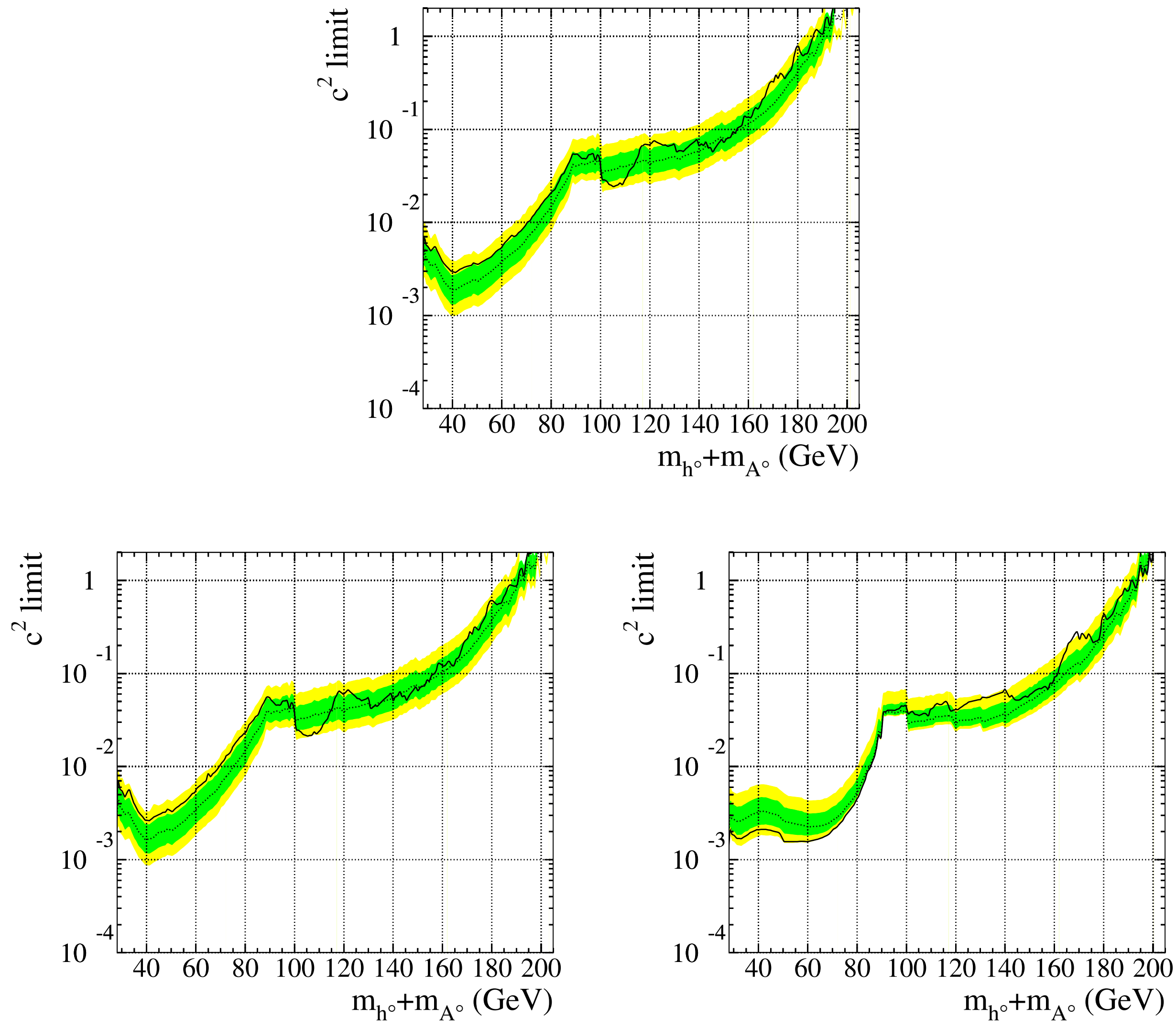

Figure 3: *Model-independent 95% c.l. upper bounds, S_{95}, for various topological cross sections motivated by the pair-production process* $e^+e^-\rightarrow\mathcal{H}_2\mathcal{H}_1$*, for the particular case where* $m_{\mathcal{H}_2}$ *and* $m_{\mathcal{H}_1}$ *are approximately equal. Such is the case, for example, in the CP-conserving MSSM scenarios for* $\tan\beta$ *greater than 10. The abscissa represents the sum of the two Higgs boson masses. The full line represents the observed limit. The dark (green) and light (yellow) shaded bands around the median expectation (dashed line) correspond to the 68% and 95% probability bands. (a) The Higgs boson decay branching ratios correspond to the* m_h*-max benchmark scenario with* $\tan\beta$*=10, namely 94%* $\mathcal{H}_1\rightarrow b\bar{b}$*, 6%* $\mathcal{H}_1\rightarrow\tau^+\tau^-$*, 92%* $\mathcal{H}_2\rightarrow b\bar{b}$ *and 8%* $\mathcal{H}_2\rightarrow\tau^+\tau^-$*)=0.08. (b) Both Higgs bosons are assumed to decay exclusively to* $b\bar{b}$*. (c) The Higgs bosons are assumed to decay, one into* $b\bar{b}$ *only and the other one into* $\tau^+\tau^-$ *only. *** It would be nice to have this plot also for* $\tau^+\tau^-\tau^+\tau^-$*. Also, the legend of the ordinate should be changed to* S_{95} ****)*

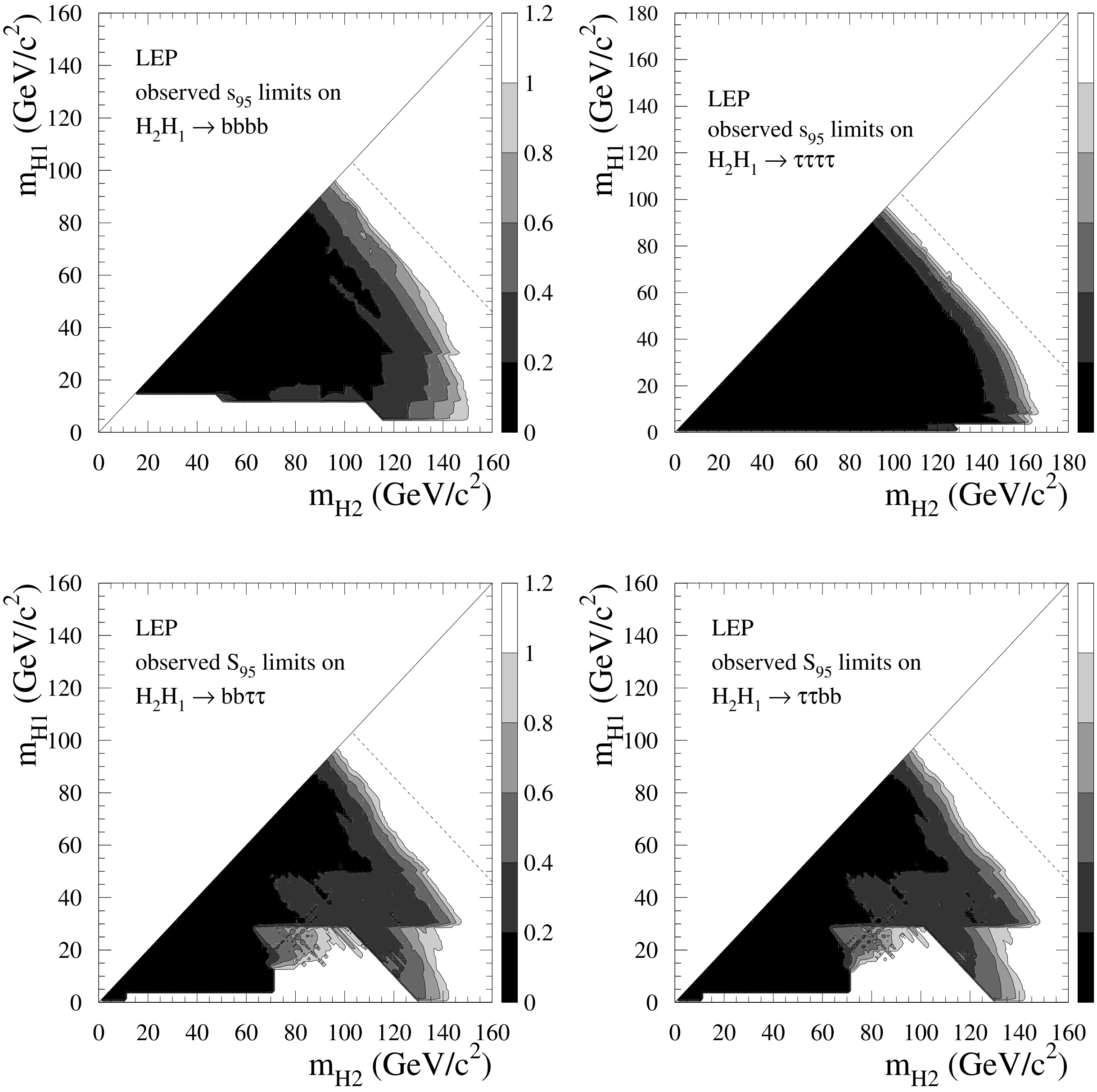

Figure 4: *Contours of the model-independent 95% c.l. upper bound, S_{95}, for various topological cross sections motivated by the pair production process* $\mathrm{e^+e^-}\to\mathcal{H}_2\mathcal{H}_1$*, projected onto the* ($m_{\mathcal{H}_2}$, $m_{\mathcal{H}_1}$) *plane. (a) Both Higgs bosons are assumed to decay to* $\mathrm{b\bar{b}}$*. (b) Both Higgs bosons are assumed to decay to* $\tau^+\tau^-$*. (c) The* $\mathcal{H}_2$ *boson is assumed to decay to* $\mathrm{b\bar{b}}$ *and the* $\mathcal{H}_1$ *boson to* $\tau^+\tau^-$*. (d) The* $\mathcal{H}_1$ *boson is assumed to decay to* $\mathrm{b\bar{b}}$ *and the* $\mathcal{H}_2$ *boson to* $\tau^+\tau^-$*.*

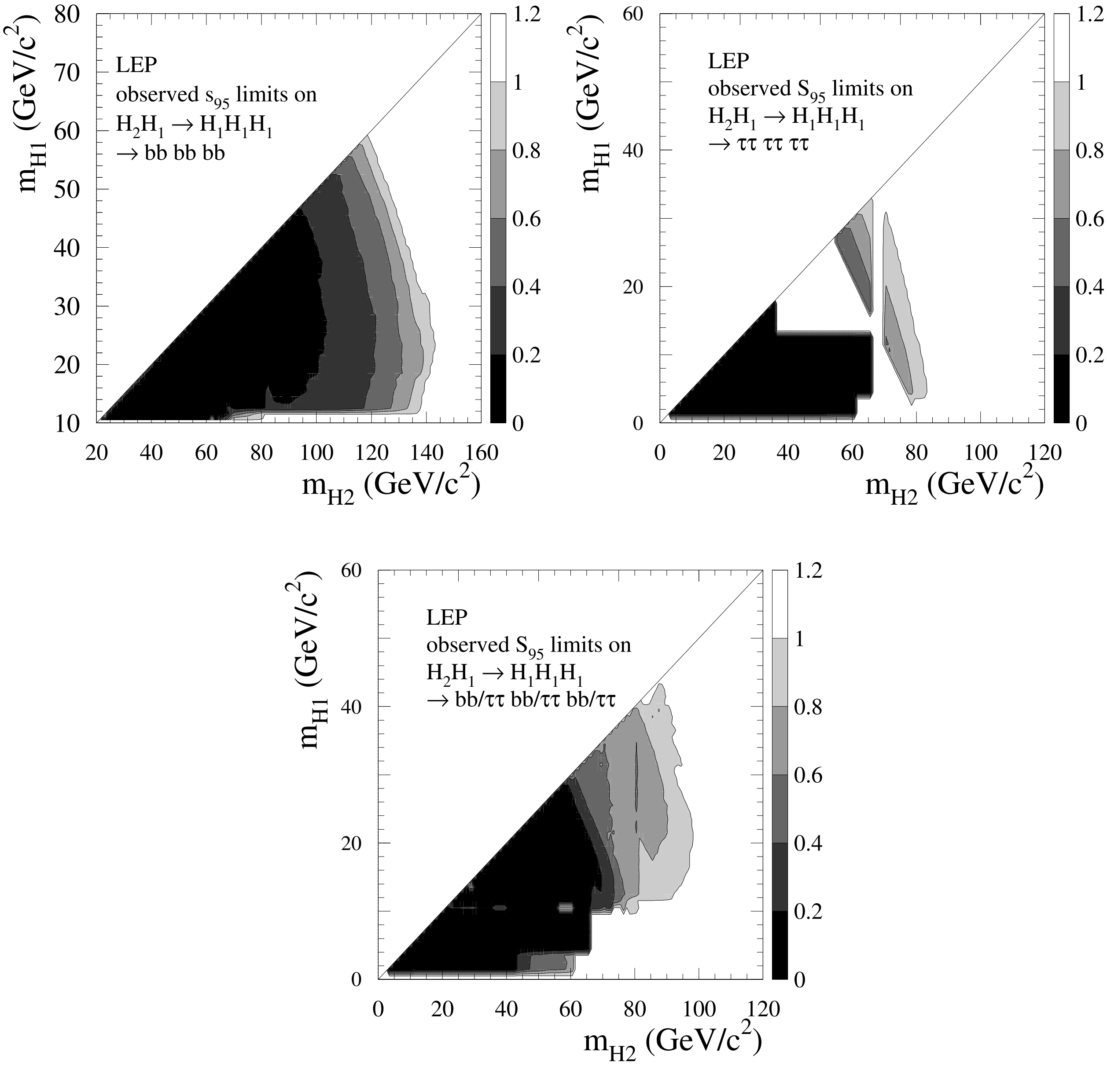

Figure 5: *Contours of the model-independent 95% c.l. upper bound, S_{95}, for various topological cross sections motivated by the pair-production cascade process* $e^+e^-\rightarrow(\mathcal{H}_2\rightarrow\mathcal{H}_1\mathcal{H}_1)\mathcal{H}_1$, *projected onto the* $(m_{\mathcal{H}_2}, m_{\mathcal{H}_1})$ *plane. (a) The* $\mathcal{H}_1$ *boson is assumed to decay exclusively to* $b\bar{b}$. *(b) The* $\mathcal{H}_1$ *boson is assumed to decay exclusively to* $\tau^+\tau^-$. *(c) The* $\mathcal{H}_1$ *boson is assumed to decay with equal probability to* $b\bar{b}$ *and to* $\tau^+\tau^-$.

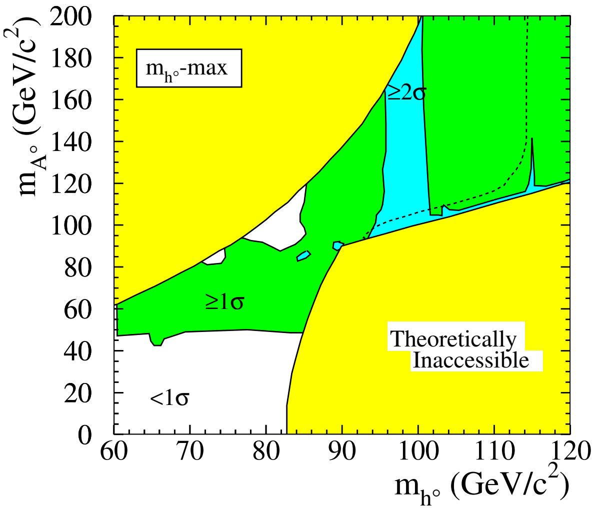

Figure 6: *Contours based on the observed p-values* $1 - CL_b$*, indicating the statistical significances of local excesses in the data. The CP-conserving MSSM benchmark scenario* m_{h}*-max is chosen for this test. The parameter space is shown in the* $(m_{\mathrm{h}}, m_{\mathrm{A}})$ *and* $(m_{\mathrm{h}}, \tan\beta)$ *projections. (*** The first plot will be extended towards low masses; the second projection will be shown too. The color codes (see below) will correspond to Fig. 15***). In the light-gray (light-green) regions the data deviate by less than one standard deviation from the expectation based on Monte Carlo simulation with no signal. Similarly, in the medium-grey (dark-green) regions the deviation is between one and two standard deviations and in the dark (blue) regions it is between two and three standard deviations. The dashed line shows the expected exclusion at 95% c.l. and represent the sensitivity limit of the present search (compare to Figure 7 below, plots (a) and (b)).*

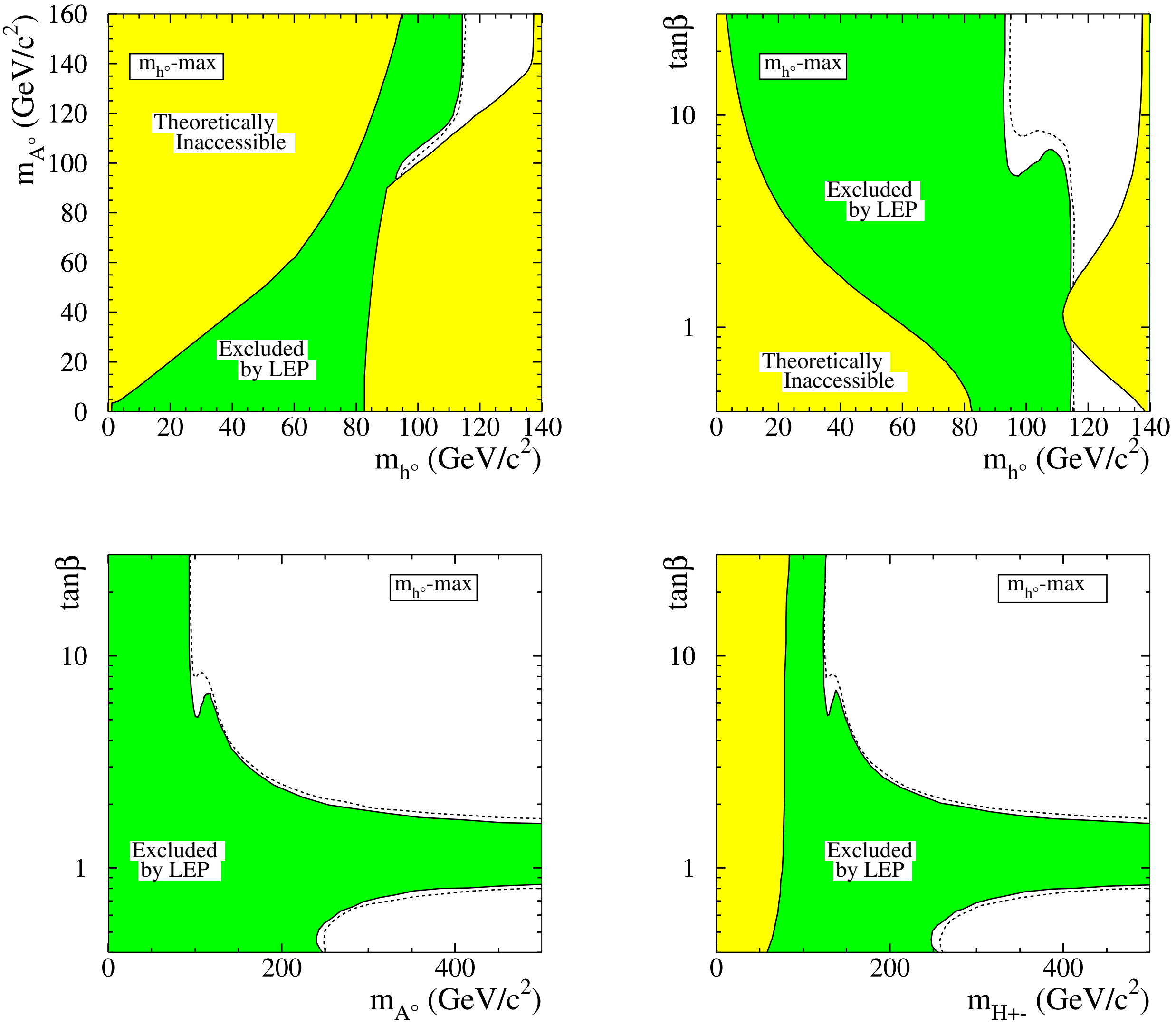

Figure 7: *The MSSM exclusions, at 95% c.l., for the $m_{\rm h}$-max benchmark scenario, with* $m_{\rm t} = 179.3\ {\rm GeV}/c^2$. *The figure shows the excluded and theoretically inaccessible regions in four projections of the MSSM parameters:* $(m_{\rm h},\ m_{\rm A})$, $(m_{\rm h},\ \tan\beta)$,$(m_{\rm A},\ \tan\beta)$ *and* $(m_{\rm H^+},\ \tan\beta)$. *The dashed lines indicate the boundaries of the regions expected to be excluded on the basis of Monte Carlo simulations with no signal. (*** It would be nice to show also the 99.7% c.l. exclusions, like in Fig. 16. Plot (b) should also show the theoretical upper bounds for* m_t *= 196.3, 174.3, 179.3 and 183.0* ${\rm GeV}/c^2$, *which is needed for the discussion of the top-mass dependence of the exclusion in* $\tan\beta$. ****)*

Figure 8: *The MSSM exclusions, at 95% c.l., for the* m_{h}*-max benchmark scenario, variant (a) (see Section 2.1.1.), with* $m_{\mathrm{t}} = 179.3\ \mathrm{GeV}/c^2$*. The figure shows the excluded and theoretically inaccessible regions as functions of the MSSM parameters in four projections: (*m_{h}*,* m_{A}*), (*m_{h}*,* $\tan\beta$*),(*m_{A}*,* $\tan\beta$*) and (*$m_{\mathrm{H^+}}$*,* $\tan\beta$*). The dashed lines indicate the boundaries of the regions expected to be excluded on the basis of Monte Carlo simulations with no signal.*

Figure 9: *The MSSM exclusions, at 95% c.l., for the* m_{h}*-max benchmark scenario, variant (b) (see Section 2.1.1.), with* $m_{\mathrm{t}} = 179.3\ \mathrm{GeV}/c^2$*. The figure shows the excluded and theoretically inaccessible regions as functions of the MSSM parameters in four projections: (*m_{h}*,* m_{A}*), (*m_{h}*,* $\tan\beta$*),(*m_{A}*,* $\tan\beta$*) and (*$m_{\mathrm{H^+}}$*,* $\tan\beta$*). The dashed lines indicate the boundaries of the regions expected to be excluded on the basis of Monte Carlo simulations with no signal.*

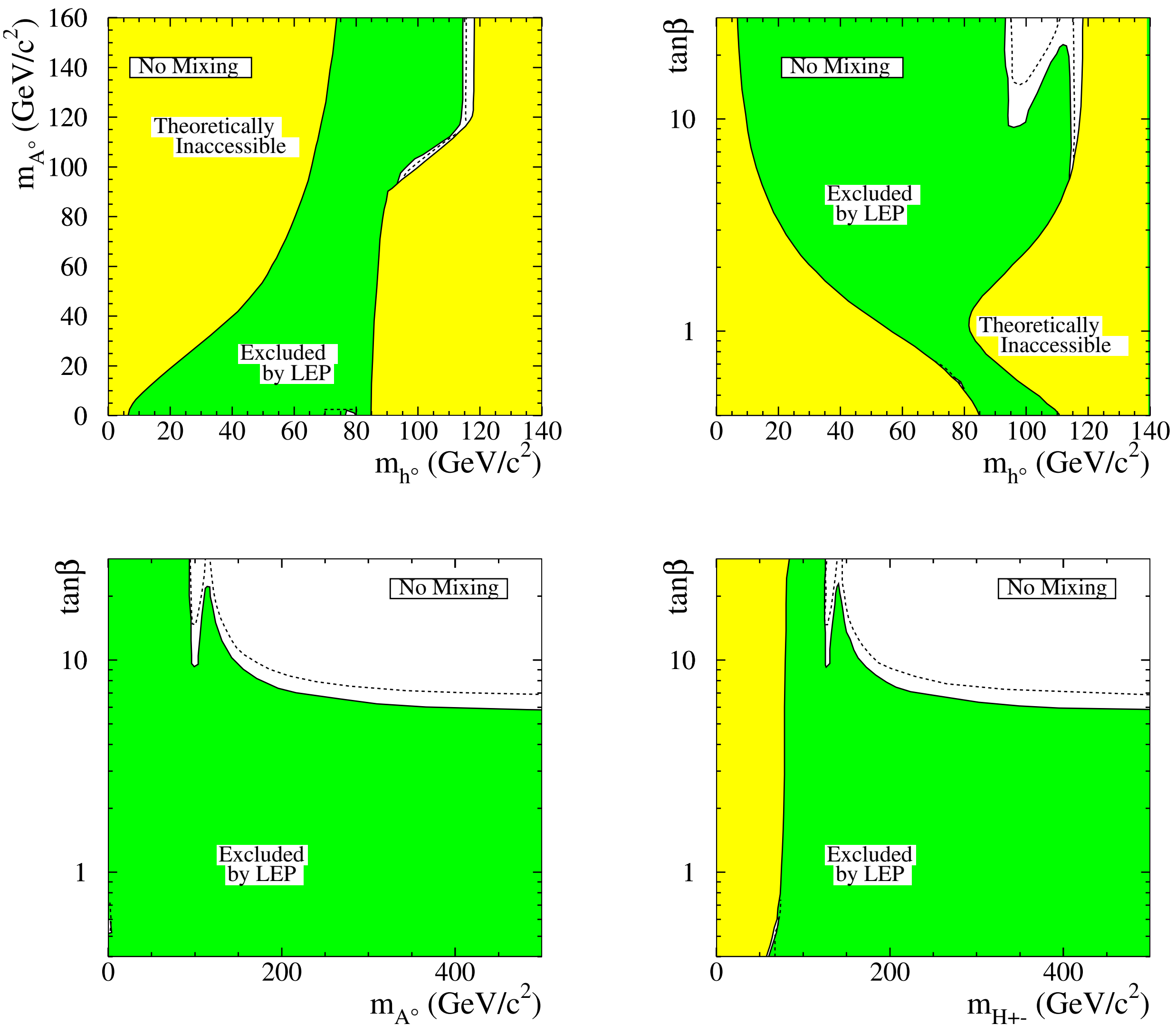

Figure 10: *MSSM parameter exclusions, at 95% c.l., for the* no-mixing *benchmark scenario, with* $m_t = 179.3$ GeV$/c^2$*. The figure shows the excluded and theoretically inaccessible regions as functions of the MSSM parameters in four projections:* $(m_h,\ m_A)$*,* $(m_h,\ \tan\beta)$*,*$(m_A,\ \tan\beta)$ *and* $(m_{H+},\ \tan\beta)$*. The dashed lines indicate the boundaries of the regions expected to be excluded on the basis of Monte Carlo simulations with no signal. (*** It would be nice to show also the 99.7% c.l. exclusions, like in Fig. 16. Plot (b) should also show the theoretical upper bounds for* m_t *= 196.3, 174.3, 179.3 and 183.0* GeV$/c^2$*, which is needed for the discussion of the top-mass dependence of the exclusion in* $\tan\beta$*. ***)*

Figure 11: *The MSSM exclusions, at 95% c.l., for the no-mixing benchmark scenario, variant (a) (see Section 2.1.2), with* $m_{\mathrm{t}} = 179.3\ \mathrm{GeV}/c^2$. *The figure shows the excluded and theoretically inaccessible regions as functions of the MSSM parameters in four projections:* (m_{h}, m_{A}), (m_{h}, $\tan\beta$),(m_{A}, $\tan\beta$) *and* (m_{H^+}, $\tan\beta$). *The dashed lines indicate the boundaries of the regions expected to be excluded on the basis of Monte Carlo simulations with no signal.*

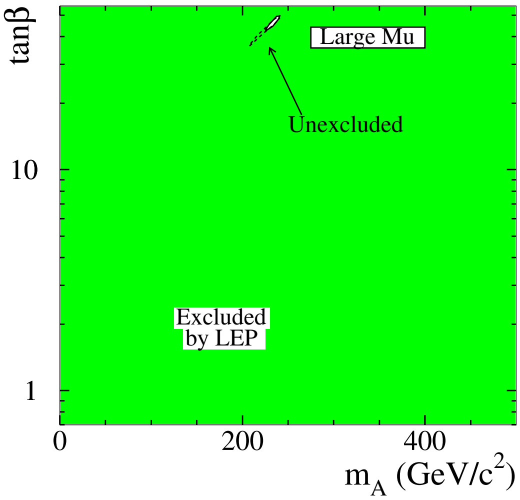

Figure 12: *The MSSM exclusion, at 95% c.l., for the large-μ benchmark scenario (see Section 2.1.3) (*** All four projections should be shown ***)*

Figure 13: *The MSSM exclusion, at 95% c.l., for the gluophobic benchmark scenario (see Section 2.1.3)*

Figure 14: *The MSSM exclusion, at 95% c.l., for the large-α_{eff} benchmark scenario (see Section 2.1.3)*

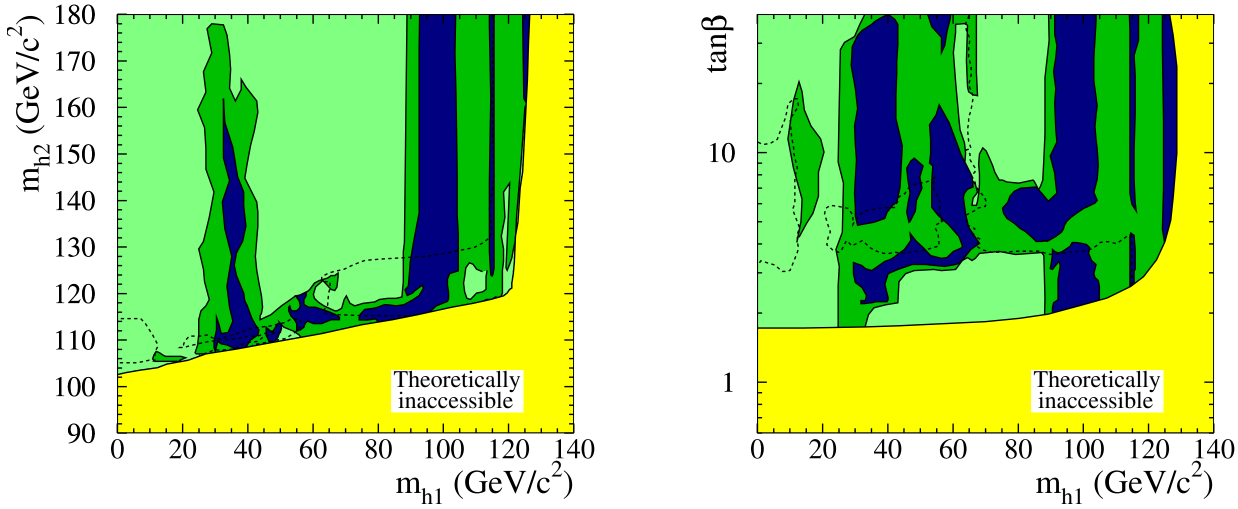

Figure 15: *Contours based on the observed p-values $1 - CL_b$ indicating the statistical significances of local excesses in the data. The CP-violating MSSM benchmark scenario CPX is chosen. The test is shown in the $(m_{\mathcal{H}_1}, m_{\mathcal{H}_2})$ and $(m_{\mathcal{H}_1}, \tan\beta)$ projections of the parameter space. In the light-gray (light-green) regions the data deviate by less than one standard deviation from the expectation based on Monte Carlo simulation with no signal. Similarly, in the medium-grey (dark-green) regions the deviation is between one and two standard deviations and in the dark (blue) regions it is between two and three standard deviations. The dashed line shows the expected exclusion at 95% c.l. (compare to Figure 16, plots (a) and (b)) and represents the sensitivity limit of the present search. CPV hotspot search.*

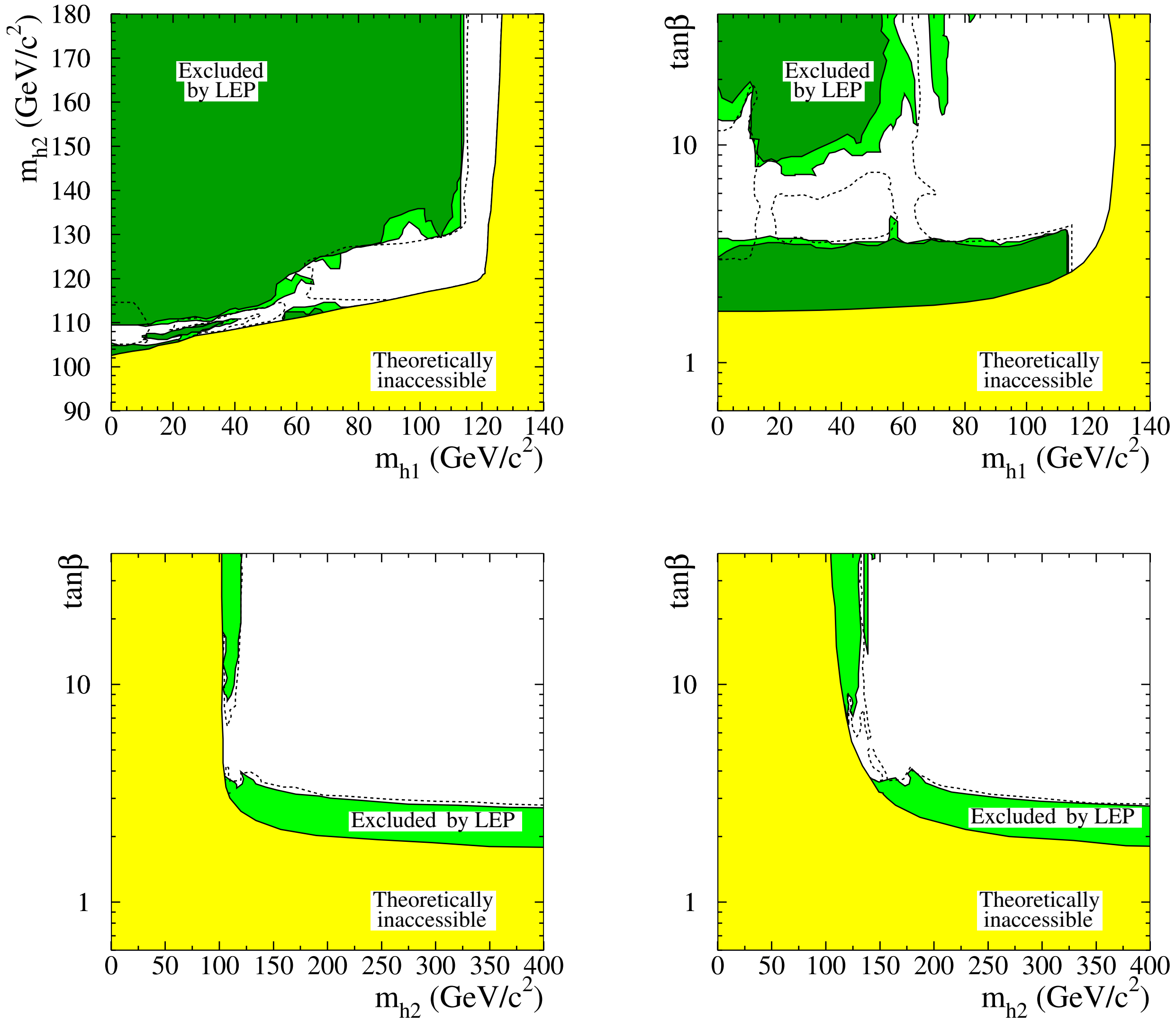

Figure 16: *Exclusions, at 95% c.l.(light-green) and 99.7% c.l. (dark-green), for the CP-violating CPX scenario with* $m_{\mathrm{t}} = 179.3\ \mathrm{GeV}/c^2$*. The figure shows the excluded and theoretically inaccessible regions as functions of the MSSM parameters in four projections:* $(m_{\mathrm{h}_1},\ m_{\mathrm{h}_2})$*,* $(m_{\mathrm{h}_1},\ \tan\beta)$*,* $(m_{\mathrm{h}_2},\ \tan\beta)$ *and* $(m_{\mathrm{H}^+},\ \tan\beta)$*. The dashed lines indicate the boundaries of the regions expected to be excluded, at the 95% c.l., on the basis of Monte Carlo simulations with no signal.*

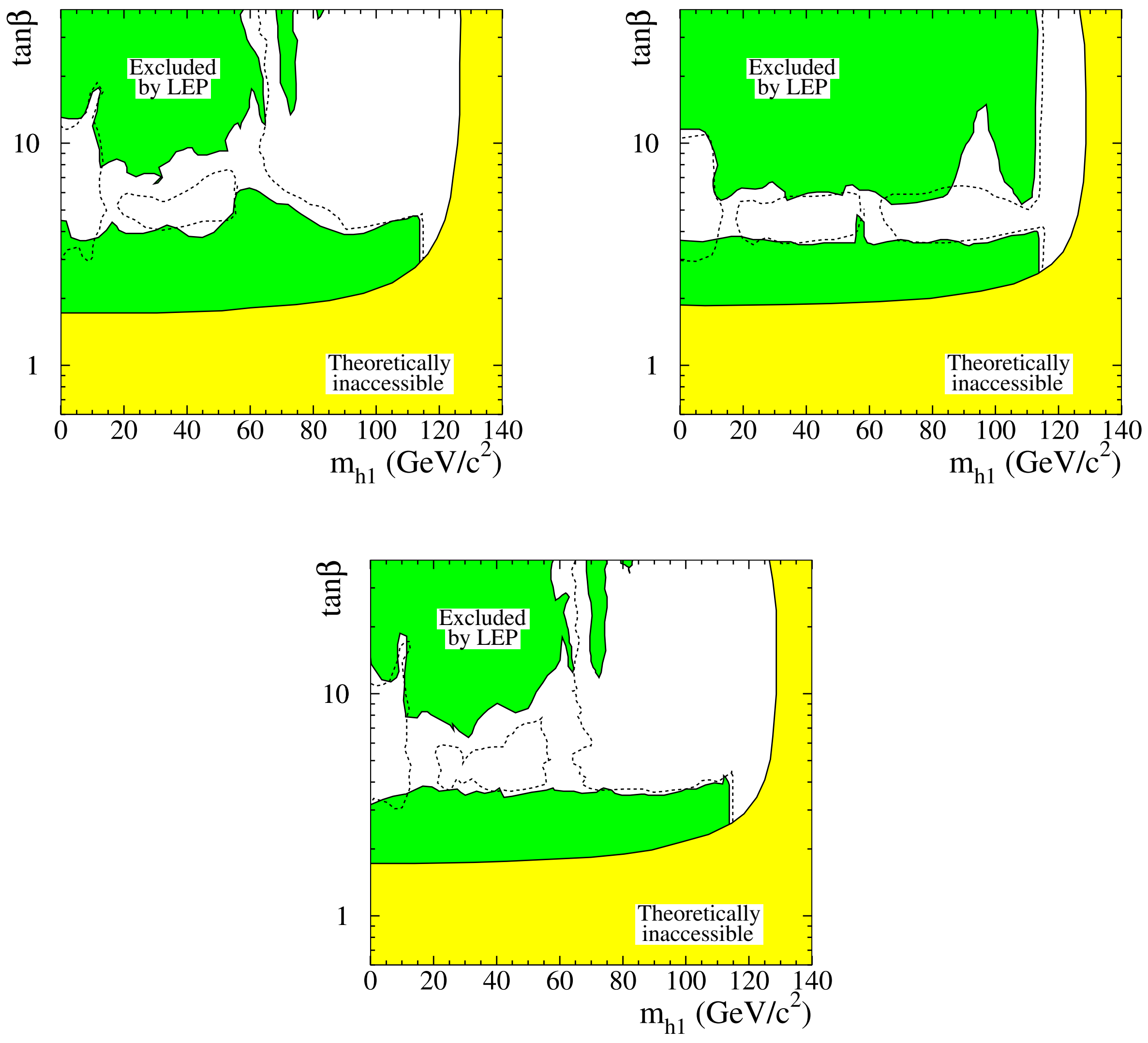

Figure 17: *Exclusions, at 95% c.l., for the CP-violating CPX scenario, for two theoretical approaches. Upper left: the CPH calculation; upper right: the FeynHiggs 2.0 calculation; lower plot: the standard procedure adopted, which means that in each point of the parameter space the calculation is chosen which provides the more conservative expected result (the lesser exclusion).*

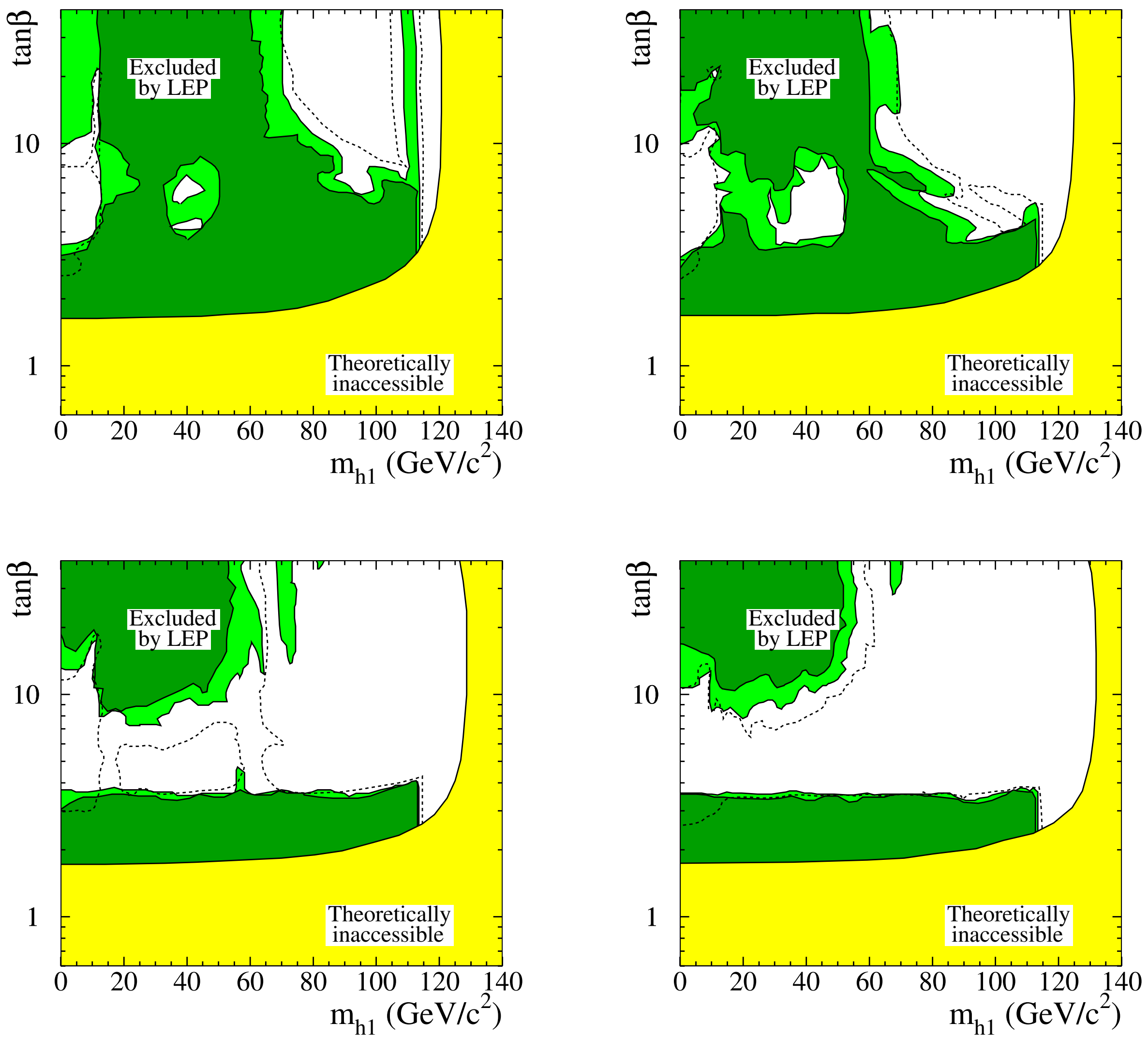

Figure 18: *Exclusions, at 95% c.l. (light-green) and at 99.7% c.l. (dark-green), for the CP-violating CPX scenario, for four top masses. From upper left to lower right:* $m_{\mathrm{t}} = 169.3\ \mathrm{GeV}/c^2$, $174.3\ \mathrm{GeV}/c^2$, $179.3\ \mathrm{GeV}/c^2$ *and* $183.0\ \mathrm{GeV}/c^2$. *In all cases and in each scan point the more conservative of the two theoretical calculations, FeynHiggs 2.0 or CPH, was used.*

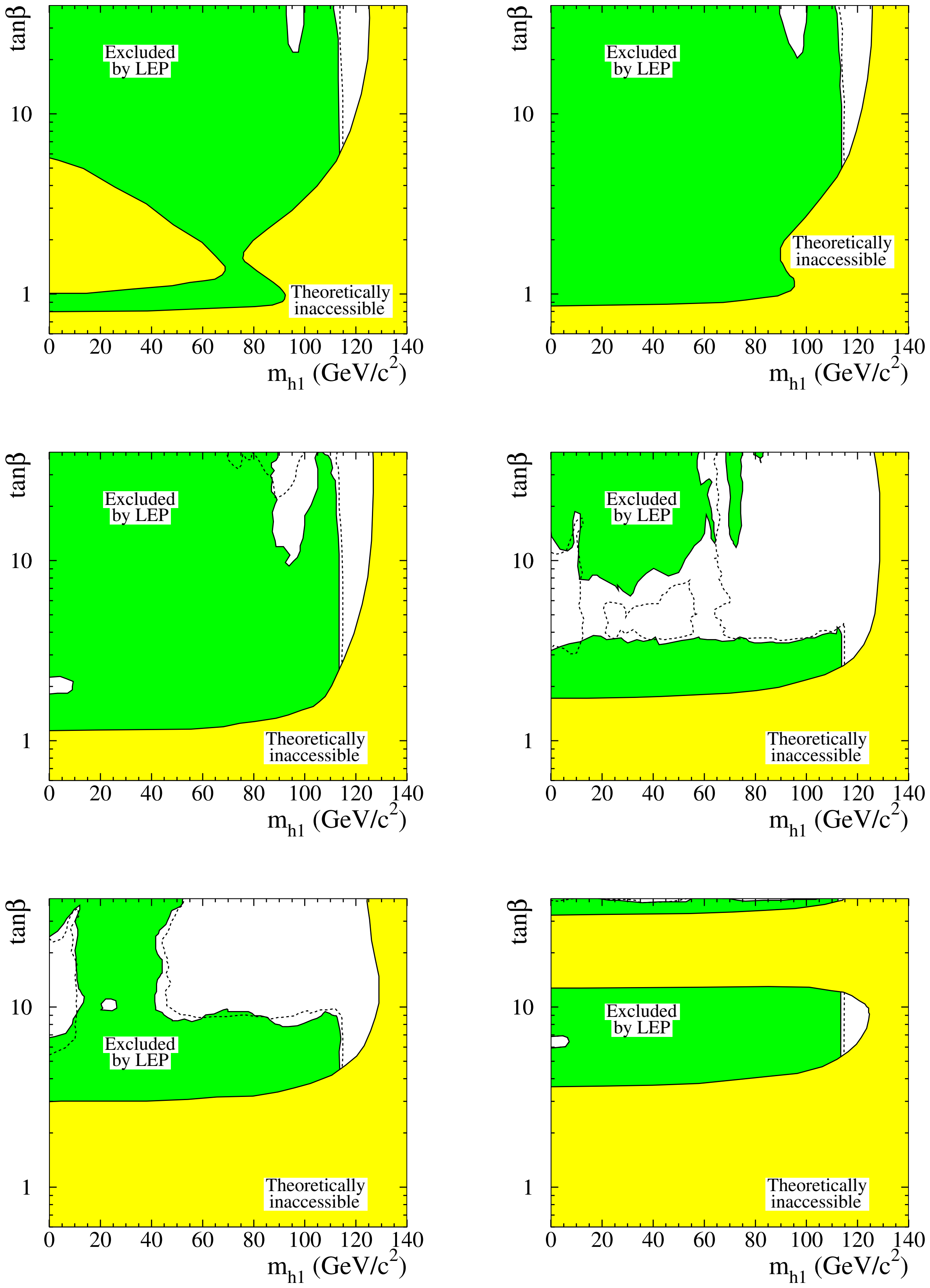

Figure 19: *Exclusions, at 95% c.l., for the CP-violating CPX scenario, for various CP-violating phases. From upper left to lower right:* 0°, 20°, 60°, 90°, 135° *and* 180°. *In all cases and in each scan point the more conservative of the two theoretical calculations, FeynHiggs 2.0 or CPH, was used.*

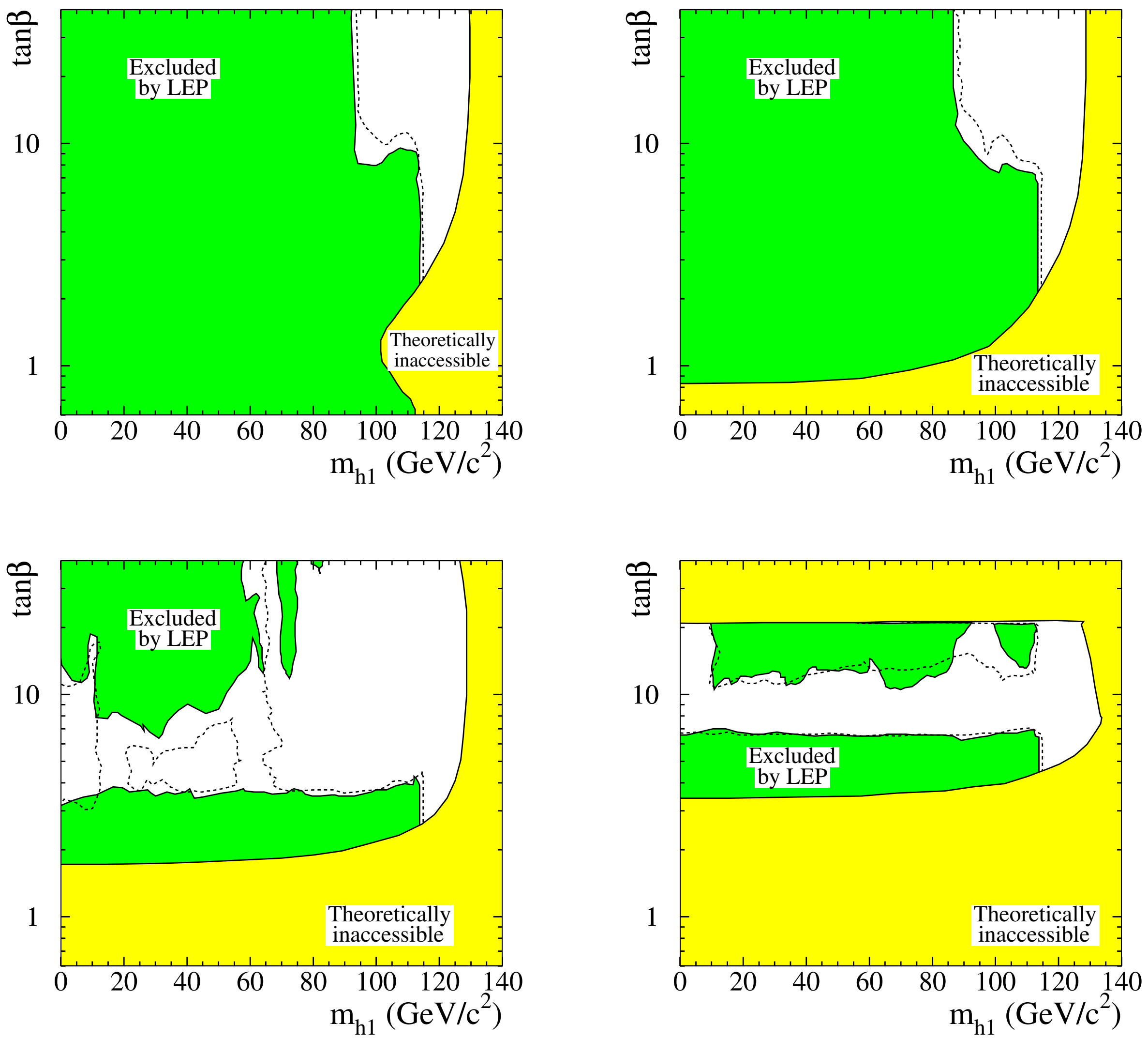

Figure 20: *Exclusions, at 95% c.l., for the CP-violating CPX scenario, for various values of the Higgs mass parameter μ. From upper left to lower right: $\mu = 500,\ 1000,\ 2000,\ 4000$ GeV. In all cases and in each scan point the more conservative of the two theoretical calculations, FeynHiggs 2.0 or CPH, was used.*

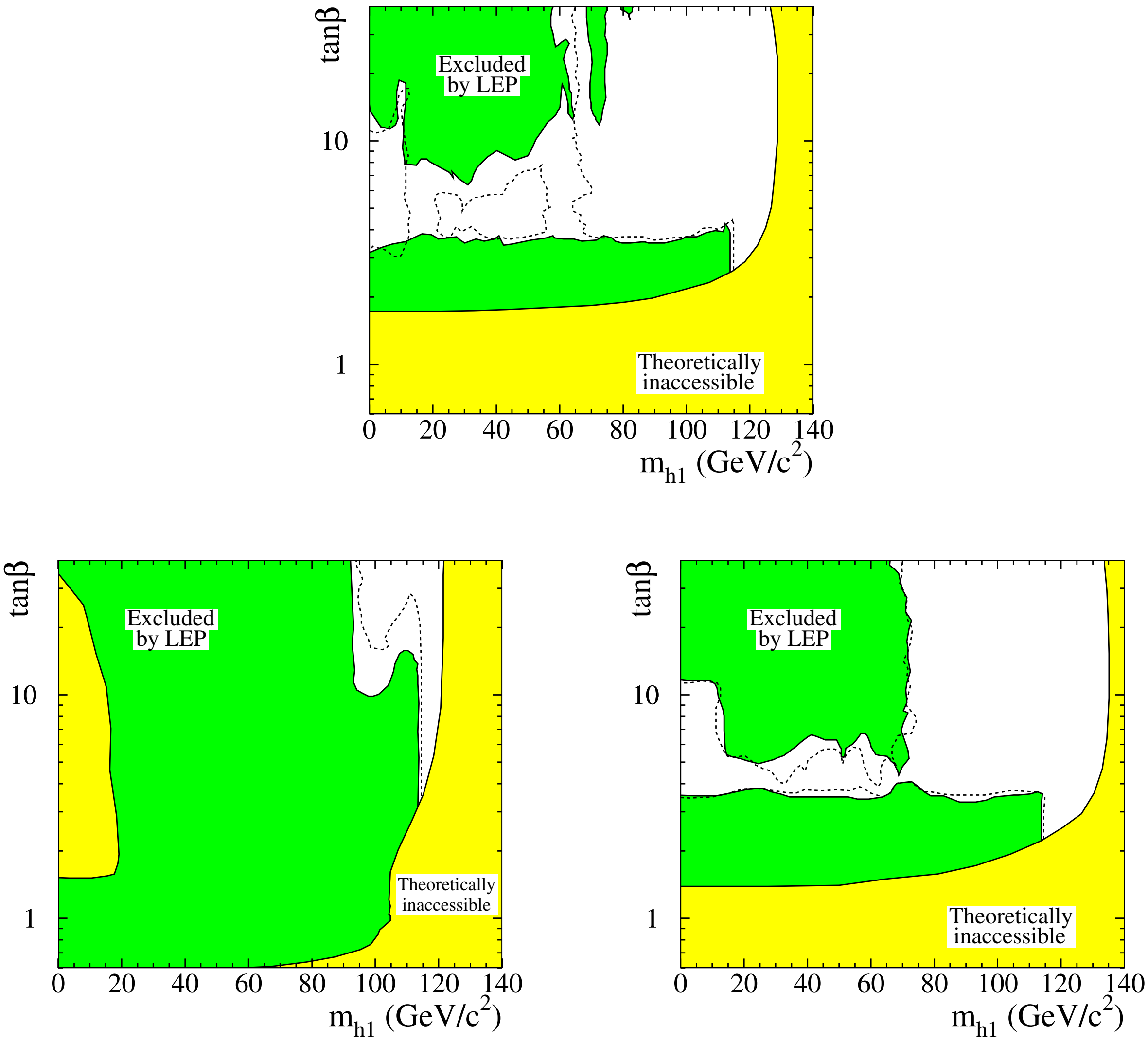

Figure 21: *Exclusions, at 95% c.l., for the CP-violating CPX scenario, for various values of the soft SUSY-breaking scale* m_{SUSY}*. Upper plot:* m_{SUSY} = 500 *GeV; lower left:* m_{SUSY} *scaled to* 1000 *GeV while all other parameters kept at the standard CPX values; lower-right:* m_{SUSY} *scaled to* 1000 *GeV but the ratios* $m_{SUSY}/|A|$ *and* m_{SUSY}/μ *are maintained at the standard CPX values. In all cases and in each scan point the more conservative of the two theoretical calculations, FeynHiggs 2.0 or CPH, was used.*